A clinically defined and xeno-free hydrogel system for regenerative medicine.

John Ong [1,2,3], George Gibbons [4], Lim Yee Siang [5], Zhou Lei [3], Junzhe Zhao [1], Alexander W. Justin [1], Federico Cammarata [1], Ravisankar Rajarethinam [6], Colleen Limegrover [4], Sanjay Sinha [7 *], Andras Lakatos [4 *], Foad J. Rouhani [8 *], Dan Yock Young [3 *], Athina E. Markaki [1 *]

** denotes senior authorship.*

[1] Department of Engineering, University of Cambridge, UK

[2] School of Clinical Medicine, University of Cambridge, UK

[3] Department of Medicine, National University of Singapore, Singapore

[4] John van Geest Centre for Brain Repair, University of Cambridge, UK

[5] Genomic Institute of Singapore, Singapore

[6] Institute of Molecular and Cell Biology, Singapore

[7] Cambridge Stem Cell Institute, University of Cambridge, UK

[8] Wellcome Sanger Institute, Wellcome Genome Campus, Cambridge, UK

Correspondence:

Professor Athina E. Markaki

Department of Engineering, University of Cambridge

Trumpington Street

Cambridge CB2 1PZ, United Kingdom

Tel: +44-1223 766417, Email: am253@cam.ac.uk

Dr John Ong

Clinical Lecturer in Hepatology

27 School of Clinical Medicine, University of Cambridge
28 Addenbrooke's Hospital, Hills Road
29 Cambridge CB2 0SP, United Kingdom
30 Tel: +44-1223 336700, Email: jo401@cam.ac.uk
31

32 **ABSTRACT (174/200 words)**

33 Biofabricated scaffolds facilitate bona fide cellular interactions, cell type specification,
34 and the formation of three-dimensional tissue architecture from human pluripotent
35 stem cells (hPSCs). However, poorly defined and non-clinically approved synthetic
36 biomaterials greatly hinder the translation of lab-grown therapies into clinical practice.
37 Here, we describe a protein screen-based hydrogel system biofabricated from widely
38 available clinical-grade human components. We show that "Alphagel", a base hydrogel
39 comprising human embryonic matrices, supports the trilineage differentiation of
40 hPSCs into neural, cardiac, and liver tissue. Alphagel is also biocompatible and
41 biodegradable *in vivo*. Further, by adding select proteins found in the maturing human
42 foetal liver, the resulting hydrogel (termed "Hepatogel") enhances the differentiation of
43 hPSC-derived hepatocytes (H-iHeps) compared to Matrigel, a xenogenic and
44 commonly used hydrogel that is prohibited in clinical use. Importantly, when injected
45 into mice livers, Hepatogel significantly improves the engraftment rates of H-iHeps
46 compared to standard cell injections. Altogether, our results provide proof of concept
47 that this customisable hydrogel system is a useful tool for developing organ-specific
48 and clinically translatable therapies for regenerative medicine and tissue engineering.

49 **Keywords:** hydrogel, liver, stem cells, regenerative medicine, tissue engineering

50 **INTRODUCTION**

51 Three-dimensional (3D) stem cell and organoid platforms recapitulate *in vivo* cellular
52 and biomechanical interactions better than two-dimensional culture systems, enabling
53 the development of novel diagnostics and therapeutics for disease (1,2). The spatial
54 arrangement of stem cells and niche factors orchestrated by biofabricated scaffolds
55 promote the self-organisation of cell masses and the formation of early organoids for

tissue development. This geometry controls organoid patterning (3) and remains an important factor that underpins our capability to engineer whole organs in vitro. Human pluripotent stem cells (hPSC), which comprise induced pluripotent stem cells (iPSCs) and embryonic stem cells (ESCs), have the potential to generate any cell type in the human body. However, hPSC and organoid culture are heavily reliant on xenogenic matrices that often cause significant immune-related reactions when transplanted, contributing to the failure of many tissue-engineered therapies at clinical trials (4).

Presently, Matrigel and Matrigel-derived matrices are often used to culture hPSCs and organoids derived from bi- or multi-potent adult stem cells (5,6). This is problematic because of widely recognised problems with the mouse sarcoma-derived matrix. Poor definability (7,8), batch-to-batch variability in growth factor concentrations (9,10), composition (11) and physical properties (10), immunogenicity (12), and pathogen transmission (13) are widely recognised issues that prevent clinical translation (14). Alternatively, synthetic biomaterials such as polyethene glycol (PEG), polyacrylic acid (PAA), polycaprolactone (PCL), or polyacrylamide (PAAm) have been explored (15). However, PEG-based biomaterials can have rapid reaction kinetics, resulting in inhomogeneous hydrogels (16). PAA hydrogels are mechanically weak, which limits their use as scaffolds in tissue engineering (17). PCL hydrogels exhibit poor cell adhesion and involve toxic reagents during synthesis (18). PAAm hydrogels require complex chemical or photo-crosslinking (19), precluding gelation and retention at target sites for convenient and effective cell delivery (7,20). Importantly, synthetic biomaterials frequently lack the physiological niche factors which, while avoiding unwanted matrix interactions, also lack the biochemical cues for efficient hPSC culture and differentiation (15,21).

Recently, attempts have been made to deconstruct components of Matrigel and conjugate these with various polymeric backbones (22,23). However, these are unsuitable for hPSC culture because some components adversely affect stem cell pluripotency by causing predilection or spontaneous differentiation towards particular lineages (24–26). For example, Laminin 111, a major component of Matrigel, promotes epithelial-to-mesenchymal transition in human ESCs by the α3β1-integrin/extracellular matrix metalloproteinase inducer complex (25).

89 To address these issues, we biofabricated a xenofree and clinically compatible system
90 mimicking the stages of embryonic development and organogenesis. We
91 hypothesised that hPSC-derived target cells would resemble primary cells closer when
92 cultured in customised hydrogels with organ-specific matrices instead of generic
93 biomaterials like Matrigel or synthetic hydrogels. In that vein, we aimed to biofabricate
94 a liver extracellular matrix (ECM)-specific hydrogel as a proof-of-concept. Through a
95 reductionist approach, we performed a focused protein screen and created a base
96 hydrogel (termed "Alphagel") that supported hPSC culture and trilineage differentiation
97 in 3D. We then added select proteins found in maturing liver ECM to Alphagel. The
98 resulting hydrogel, termed "Hepatogel", produced hPSC-derived hepatocytes that
99 were closer to maturing human hepatocytes than Matrigel, and it improved the
100 engraftment of hPSC-derived hepatocytes when injected into the livers of
101 immunocompromised mice. A summary of the workflow is illustrated in Fig.1(A).
102 Herein, we contribute evidence that organ-specific hydrogels produce better end-
103 target cells than generic hydrogels, and this system is a useful tool for developing
104 organ-specific and effective therapies for regenerative medicine.

105

106 **RESULTS**

107 **Focused screening revealed Laminin 521 and Fibrinogen as common**
108 **components of the embryological and hepatic niche that contribute to hPSC**
109 **pluripotency.**

110 We previously (27) exposed iPSCs maintained on vitronectin in a defined feeder-free
111 system to a library of proteins identified within the adult human liver by the Human
112 Matrisome Project (http://matrisomeproject.mit.edu; Massachusetts Institute of
113 Technology, USA). In doing so, we were able to long-list hepatic matrix proteins that
114 enhance the *in vitro* differentiation of iPSCs to adult hepatocytes when exposed to
115 hepatic differentiation factors(27). However, to biofabricate a hydrogel that can support
116 PSC expansion seen in embryogenesis and liver organogenesis, we first investigated
117 whether any of the long-listed proteins could also maintain PSC pluripotency in the
118 absence of routine hepatic differentiation factors. Successful hits could then be used
119 as components to biofabricate a hydrogel that is primed for liver tissue engineering
120 when hepatic differentiation conditions are introduced. To that end, we optimised an

121 automated high throughput imaging pipeline to identify PSCs by nuclear area and
122 nuclear markers of stem cell pluripotency (NANOG, SOX2, and OCT4). Cell
123 morphology and the mean fluorescent intensities (MFI) of pluripotency markers were
124 used to define normal hPSC characteristics for positive selection; Supplementary
125 Figure 1. Human fibroblasts were used for threshold setting (negative control).
126
127 Using machine learning, the pipeline successfully identified pluripotent hPSCs as
128 single cells growing in 2D colonies with a sensitivity of 89.5% and a positive likelihood
129 ratio of 160.8, e.g. Fig.1(B). Single-cell analyses were performed to exclude culture
130 artefacts and cell clumps which reduce the accuracy of automated image analysis.
131 The pipeline also identified non-pluripotent cell populations with a specificity of 99.4%
132 and a negative likelihood ratio of 0.1), e.g. Fig.1(C). The final readout of the pipeline
133 was the Stemness Index (SI), a ratio of the number of pluripotent cells to the total
134 number of cells identified by DAPI. The SI ranged from 0, denoting the poorest
135 performing matrix at maintaining hPSC pluripotency, to 1, denoting pluripotency was
136 maintained in all hPSCs cultured in a matrix. Importantly, it reliably discriminated
137 between undifferentiated hPSCs and differentiated hPSCs within the same cell
138 population; Fig.1(D). When tested, this platform demonstrated excellent discriminatory
139 performance (Area Under the Curve (AUC) of 0.977); Fig.1(E).
140
141 Using this platform, we screened twenty-two proteins over a thousand conditions and
142 found select proteins in both the embryological and fetal liver niches that affect hPSC
143 pluripotency. An example of a short-term (1-week) focused screening panel is
144 illustrated in Supplementary Figure 2. In summary, the best candidate was chosen for
145 its ability to maintain the highest SI in hPSCs after prolonged culture; Laminin 521 had
146 the highest SI (between 0.95 to 1.0) after 3-4 months in culture. Thus, we sought to
147 combine Laminin 521 with a polymeric backbone to obtain a 3D scaffold since a pure
148 or physiologically relevant Laminin 521 hydrogel is not currently available. We found
149 human fibrinogen was the most suitable polymeric protein for pairing with Laminin 521
150 because of its mechanical tunability, and at low concentrations, it did not cause rapid
151 spontaneous differentiation of hPSCs (SI: 0.77 to 0.84). Notably, other polymeric
152 backbones, such as albumin and collagen, that we investigated either resulted in poor
153 hPSC attachment (27) or triggered significant spontaneous differentiation of hPSCs
154 (SI < 0.5); examples are shown in Supplementary Figure 3. In summary, in our focused

155 screen, Laminin 521 and fibrinogen showed high SIs, supporting stem cell pluripotency
156 and 2D expansion in vitro. Thus, we biofabricated a hydrogel using these two
157 candidates as base components.
158
159 **Fibrinogen and Laminin concentrations inversely affected hPSC growth in 3D.**
160 To determine the optimum conditions for culturing hPSCs in 3D, we evaluated different
161 compositions of Laminin 521-enriched fibrin hydrogels (FLGs) versus fibrin hydrogels
162 (FGs) as controls. We found that both categories of hydrogels displayed distinctive
163 characteristics. In 2D cell culture, cell attachment and expansion were significantly
164 better in FLGs (70-100% confluence) versus FGs (10%-20% confluence) after 4-5
165 days in culture, Fig.2(A). This was reflected in the average fold increase in cell
166 populations at 7 days (38.5 ± 5.6 vs 1.0 ± 0.2, $p < 0.0001$), respectively. In 3D cell
167 culture, higher fibrinogen and lower laminin concentrations resulted in poor colony
168 expansion and "dark" unhealthy hPSC colonies, Fig.2(B); widely recognised features
169 of spontaneous differentiation in hPSC culture (28–30). This was corroborated across
170 several conditions by a significant decrease in SOX2, NANOG, OCT4 MFIs, and SIs
171 compared to hPSCs grown on 2D Matrigel as standard practice (Supplementary
172 Figure 4). Nonetheless, the optimal balance between fibrinogen, thrombin and laminin
173 concentrations was identified by a combination of SI in hPSCs and the stability of FLGs
174 in cell culture; hydrogels with low fibrin concentrations (≤ 1mg/ml) disintegrated after
175 a week in cell culture. This optimum ratio (50%:50% v/v Laminin 521 and 2.5mg/ml
176 fibrin hydrogel) was termed "Alphagel". Alphagel was found to be up to a third more
177 cost-effective than Matrigel for 3D hPSC cell culture (Supplementary Figure 5). Unlike
178 other compositions of FLGs, Alphagel supported the healthy expansion of hPSCs into
179 3D cell aggregates closely resembling embryoid bodies (EBs), Fig.2(B).
180
181 To visualise the differences between fibrin-only hydrogels and Alphagel, scanning
182 electron microscopy (SEM) was performed on acellular hydrogels. This demonstrated
183 smaller pores and thinner fibrin fibres as previously observed in laminin-fibrin
184 hydrogels (31,32). Thin membranes in between inter-connecting fibrin fibres in
185 Alphagel were observed and these were absent in fibrin-only hydrogels; Fig.2(C) and
186 Fig.2(D). As protein concentration alters the elastic properties of hydrogels, we next
187 measured Young's modulus of fibrin-only hydrogels, FLGs, and Alphagel. We found
188 that hydrogel stiffness increased significantly with laminin and fibrin concentrations;

189 Fig.2(E). The Young's modulus in FLGs containing 1.5 mg/ml fibrin was higher
190 compared to 1.5 mg/ml fibrin-only hydrogels (fold increase 3.6 ± 0.6, $p < 0.0001$) and
191 2.5 mg/ml fibrin-only hydrogels (fold increase 2.6 ± 0.2, $p < 0.0001$). Despite the
192 increase in stiffness, cell viability was notably higher in Alphagel compared to fibrin-
193 only hydrogels (98.7 ± 0.3% vs 80.8% ± 8.3% respectively, $p <0.05$); Fig.2(F). There
194 were no significant differences in cell viability across Alphagel and the 2D substrates.
195
196 Next, to determine if the FLG hydrogels were stable, we measured the amount of
197 Laminin 521 leached from acellular Alphagel into the culture media over time. This
198 showed that the greatest loss of Laminin 521 from the hydrogel occurred during the
199 first 24 hr of conjugation (approximately 3% leached into media). Thereafter, the
200 leaching of Laminin 521 into the culture media was negligible, and approximately 97%
201 of the laminin remained within the hydrogel after 9 days; Fig.2(G) and Fig.2(H). Then,
202 to optimise 3D culture conditions, we tested the performance of hPSC-laden Alphagel
203 paired with different stem cell maintenance media over 2 months. Stem cell culture
204 media E8™, TeSR-E8 ™, mTeSR™ 1, mTeSR™ Plus, and TeSR™ 2 were used. We
205 found the best stem cell culture media that maintained markers of hPSC pluripotency
206 with Alphagel were the TeSR-only family i.e. TeSR™ 2, mTeSR™ 1 and mTeSR™
207 Plus, yielding SIs of hPSCs between 0.95 to 1.0; Supplementary Figure 4. Despite
208 prolonged culture, pluripotency markers (OCT4, NANOG, and SOX2) were still
209 strongly expressed in the 3D hPSCs aggregates. For validation, these aggregates
210 were dissociated into smaller cell clusters and grown as a single cell layer in 2D.
211 Importantly, these hPSCs continued to proliferate in 2D and continued to express all
212 3 pluripotent nuclear markers (Supplementary Figure 6). In summary, Alphagel was
213 found to be a stable hydrogel that supports the formation and expansion of embryoid-
214 like bodies in prolonged 3D hPSC culture, displaying different biological and physical
215 characteristics compared to fibrin-only hydrogels.
216
217 **Alphagel supported the tri-lineage differentiation of hPSC bodies into cardiac,**
218 **neural, and hepatic tissue in 3D.**
219
220 To rigorously demonstrate that hPSCs cultured in Alphagel remained pluripotent, we
221 cultured hPSCs bodies in Alphagel then performed directed 3D differentiation of

222 hPSCs into all three germ cell lines: mesoderm (cardiac), ectoderm (neurons), and
223 endoderm (hepatic).
224
225 During cardiac specification, hPSC bodies in Alphagel successfully proliferated and
226 formed 3D contractile cardiac tissue after initiating cardiac differentiation; Fig.3(A) and
227 Supplementary Movie 1. Immunofluorescent staining (IF) of cells for the cardiac
228 marker Troponin T (TnT) and the general myoblast marker α-SMA (33) was strongly
229 positive; Fig.3(B). Cardiomyocytes were observed to start beating at a rate of 30 to 50
230 beats/min between Day 5 to Day 8 of the cardiac differentiation process; early
231 contractions were weak and asynchronous (Supplementary Movie 1). However, the
232 contractility rate increased to 60 — 80 beats/min, and contractions were noticeably
233 stronger and synchronous by Day 12 — 14 (Supplementary Movie 2). There was no
234 significant difference in differentiation efficiency (proportion of TnT positive cells)
235 between Alphagel and Matrigel (75.4 ± 18.5% vs 78.2 ± 15.4% respectively, $p = 0.14$).
236 In fibrin-only hydrogels, the differentiation efficiency was significantly lower versus
237 Alphagel (34.9 ± 21.3%; $p < 0.001$); Supplementary Figure 7(A).
238
239 For neural specification, hPSCs were subjected to a commonly applied protocol
240 utilising dual-SMAD inhibition (34,35). For comparison, both a fibrin-only control and
241 an aggregate-based (neurosphere) method were included. Neurospheres are derived
242 from hPSCs cultured with Matrigel, and then differentiated in suspension culture. At
243 Day 16, all conditions showed successful acquisition of a neural fate as demonstrated
244 by co-expression of the neuroepithelial progenitor markers SOX2, nestin, and β-
245 catenin (36); Fig.3(C). Quantifications at this time point showed comparable cell
246 composition of SOX2 immunoreactive (IR) progenitor cells in Alphagel (79.5 ± 5.0%)
247 and neurospheres (82.4 ± 9.3%) conditions. In the fibrin-only condition, there were
248 slightly fewer SOX2 IR cells (74.1 ± 12.6%); however, this difference was not
249 statistically significant; Supplementary Figure 7(B). To ascertain if the structural
250 properties of Alphagel could improve the organization and morphology of differentiated
251 neuroepithelia, we determined the number and size of lumens demarcated by
252 nestin/β-catenin co-labelled apical cells and compared to that seen in fibrin-based
253 hydrogels and neurospheres. We found that the frequency of polarized areas
254 (approximately $0.03/mm^2$) was consistent across all conditions, albeit less variable
255 under hydrogel conditions; Fig.3(D). However, the average lumen area was

256 significantly increased in hydrogel conditions with Alphagel (403.29 μm^2; $p = 0.0007$)
257 versus neurospheres (105.46 μm^2); Fig.3(D). Large lumen areas are observed when
258 neural progenitors coalesce and mature (37,38), forming the structural architecture of
259 the neural progenitor niche. The correct organisation of polarised tissue is crucial to
260 neurodevelopment, and aberrant formation is involved in neural tube defects.
261 Nonetheless, no differences were observed in the frequency of polarised puncta in
262 Alphagel versus neurospheres; Fig.3(E). Cumulatively, these results show that
263 Alphagel supports efficient ectodermal differentiation of hPSCs into neuroepithelia.
264
265 For hepatic specification, successful differentiation of hPSCs into hepatocytes (iHeps)
266 was demonstrated through IF staining, showing previously established gene
267 expression signatures (39), and functional assays. Positive IF staining for hepatocyte
268 markers Albumin, HNF1A, HNF4A, CYP2A6, CD147, and E-cadherin was
269 demonstrated in 3D differentiated cells, Fig.4(A). Similarly, key hepatocyte genetic
270 markers HNF4A, CEBPA and CYP3A4 were shown to be expressed in iHeps derived
271 in Alphagel and at similar levels as iHeps derived in Matrigel; Fig.4(B). However,
272 CYP3A7 and AFP expression were significantly higher in Alphagel and Matrigel
273 compared to adult primary human hepatocytes (PHH); $p < 0.0001$ for both, Fig.4(B).
274 Notably, TBX3 expression was also high in Alphagel and Matrigel but there was no
275 statistically significant difference compared to PHH. For further characterisation, 18
276 other hepatocyte-related genes were analysed (Supplementary Figure 8). 10 of 18
277 genes showed differences between PHH and Alphagel-derived hepatocytes.
278 Specifically in the latter, BAAT, ABCC2, and TAT were down-regulated, whilst
279 CYP3A5, GATA4, GATA6, FOXA1, SOX9, LGR5, and CK19 were up-regulated
280 compared to PHH (p values in Supplementary Figure 8). BAAT and TAT code for liver
281 enzymes and ABCC2 is a cell-membrane transporter. CYP3A5 codes for a hepatic
282 enzyme that increases as the foetal liver matures. GATA4, GATA6, FOXA1 are
283 important transcription factors involved in hepatic differentiation. LG5R and SOX9 are
284 markers for hepatic progenitors (hepatoblasts) that give rise to the two main cell types
285 within the liver (hepatocytes and cholangiocytes). CK19 is a biliary marker.
286
287 To assess the functionality of iHeps derived in Alphagel, albumin secretion,
288 cytochrome 3A4 activity, LDL update, as well as CDFDA uptake and excretion were
289 investigated at the end of the hepatic differentiation process. Albumin, a key marker

290 of hepatocyte synthetic function (40), was found to be secreted in similar amounts by
291 PHH and iHeps cultured in Alphagel and Matrigel; Fig.4(C). However, CYP3A4 activity
292 was lower in Alphagel and Matrigel than PHH, as reported by other groups (39,41);
293 Fig.4(D). Importantly, low-density lipoprotein (LDL) uptake and 5-(and-6)-Carboxy-
294 2',7'-Dichlorofluorescein Diacetate (CDFDA) secretion, both features of hepatocyte
295 metabolic function, were demonstrated in Alphagel; Fig.4(E) and Fig.4(F). These were
296 also present in primary hepatocytes and hepatocytes derived in Matrigel. There was
297 no statistically significant difference in differentiation efficiency between Alphagel and
298 Matrigel (defined herein by the proportion of albumin-positive cells). This was
299 approximately 70.6% and 69.9%, respectively ($p=0.73$). In fibrin-only hydrogels, the
300 differentiation efficiency was significantly lower versus Alphagel (28.8%, $p<0.0001$);
301 Supplementary Figure 7(C).
302
303 In summary, the results above show that Alphagel maintains hPSCs pluripotency and
304 supports their trilineage differentiation in 3D. Using established and chemically defined
305 differentiation protocols, cardiac, neural, and hepatic tissue were derived in 3D and
306 positively characterised.
307
308 **Alphagel demonstrated good biocompatibility and biodegradability *in vivo***
309 To explore if Alphagel could be used as a biomaterial for clinical therapy, we next
310 sought to determine its biocompatibility *in vivo*. To that end, we injected immune-
311 competent Black 6 (C57BL/6) mice subcutaneously with Alphagel (test group), 0.9%
312 saline (negative control), and 1.0% v/v croton oil (inflammatory agent, positive control)
313 to assess for an immune response; n=3 for each group and time point. Mice were then
314 observed and culled over 6 weeks. Histological slides were evaluated by a veterinary
315 histopathologist who was blinded to the groups. Each slide was scored objectively
316 using an international scoring tool (Supplementary Figure 9) and graded using
317 standardised nomenclature (42–44).
318
319 Cumulatively, the results showed that mice injected with Alphagel had mild
320 inflammation at the site of injection between 1 to 2 weeks; Fig.5(A). However, this
321 resolved completely between 4 to 6 weeks; Fig.5(B). Mice injected with 0.9% saline
322 also had inflammation at the injection site after 1 week although this was minimal and
323 had resolved completely by 2 weeks. Mice injected with 1% croton oil developed

ongoing severe inflammation, which progressed to wound dehiscence by 6 weeks; these mice were culled humanely when wound inflammation became visibly severe. The histological scores were consistent with the qualitative reporting of the histological slides, Fig.5(C).

Neoplasia was not observed at the injection sites in all groups, and Alphagel was not visible at the injection sites between 4 to 6 weeks. In summary, the data derived from immunocompetent Black 6 mice provide evidence that fibrin-laminin hydrogels are biocompatible and biodegradable *in vivo*.

Alphagel enriched with liver-specific ECM (Hepatogel) enhanced the phenotype of human iHeps

To test our hypothesis that hydrogels enriched with organ-relevant ECM can improve stem cell-derived phenotypes, we added Laminin 411 and Laminin 111 to Alphagel. These were specific ECMs that we found to be important in liver development (27). Various combinations of protein concentrations were tested, and the optimum concentration of Laminins 521, 411 and 111 was termed “Hepatogel”. iHeps derived in Hepatogel, Alphagel and Matrigel were compared against PHH using the same panel of liver-specific genes and functional assays. Key changes in the gene expression profile are highlighted in Fig.6(A). Briefly, Hepatogel increased the gene expression for the hepatic glycoprotein Transferrin (TF) versus Alphagel (1.5 ± 0.4 fold increase, $p < 0.0001$) and PHH (2.2 ± 0.6 fold increase, $p < 0.001$). The gene expression for the liver enzyme Gamma Glutamyl-Transferase (GGT) was also significantly increased across all three hydrogels compared to PHH but it was highest in Hepatogel (3.3 ± 0.3 fold increase vs PHH, $p < 0.05$). Notably, gene expression for liver enzyme Glucose-6 Phosphatase (G6PC) was significantly lower in Matrigel versus PHH (-6.7 ± 0.6 fold lower, $p < 0.05$), however, expression in Hepatogel was comparable to PHH. Bipotent-hepatoblast marker LGR5 was significantly upregulated in Alphagel (6.0 ± 0.6 fold increase; $p<0.01$) and Hepatogel (6.5 ± 0.5 fold increase; $p < 0.01$) versus PHH. Importantly, expression of immature fetal liver markers CYP3A7 and AFP were significantly lower in Hepatogel versus Matrigel (1.8 ± 0.4 fold decrease; $p < 0.05$ and 1.3 ± 0.1 fold decrease; $p < 0.05$, respectively). The remaining results of the hepatocyte gene panel are attached in Supplementary Figure 10.

358 The synthetic function of hepatocytes was assessed by albumin secretion. Hepatogel
359 induced the highest albumin secretion compared to Alphagel, PHH, and Matrigel;
360 Fig.6(B). The metabolic function of hepatocytes was assessed by CYP3A4 activity and
361 Apolipoprotein B (APOB) secretion. CYP3A4 activity was highest in PHH. iHeps
362 derived in Hepatogel had higher CYP3A4 activity than Alphagel (2.4 ± 0.1 fold
363 increase; $p < 0.05$) and Matrigel. However in the latter, the increase was marginal and
364 not statistically significant (1.2 ± 0.5; $p = 0.47$), Fig.6(C). APOB secretion was higher
365 in Hepatogel compared to PHH however there were no differences between Hepatogel
366 and Alphagel (Supplementary Figure 11). In summary, the two liver-relevant ECM
367 added to Alphagel resulted in higher TF expression, CYP3A4 activity, and Albumin
368 secretion compared to Alphagel alone. Interestingly, up-titrating Laminin 411
369 concentrations in Hepatogel significantly increased APOB secretion. Conversely, this
370 promoted the formation of branching 3D tubular structures with a corresponding rise
371 in Alkaline Phosphatase (ALP) in the culture media (Supplementary Figure 11).
372 Interestingly, these structures were lined with cells which expressed biliary markers
373 CK7, CK19, and SOX9 (Supplementary Figure 12, Supplementary Movie 3 and
374 Supplementary Movie 4). In summary, we have shown that a hydrogel biofabricated
375 from hepatic niche proteins (Hepatogel), enhanced several important markers of
376 hepatocyte maturity in hPSC-derived hepatocytes compared to genetic hydrogels
377 (Alphagel and Matrigel), producing hepatic tissue in 3D.
378
379 **Hepatogel improved the engraftment of transplanted hepatocytes compared to**
380 **standard therapy.**
381 Since iHeps cultured in Hepatogel (H-iHeps) had a better synthetic (protein synthesis)
382 and metabolic profile than Alphagel, we next investigated if by introducing a
383 proliferative/regenerative liver niche at the site of transplantation, the engraftment of
384 transplanted hepatocytes could be improved. Currently, hepatocyte engraftment rates
385 in cell therapy are poor, and Matrigel and its derivatives, are not permitted in clinical
386 use (14). To that end, we injected equal quantities of H-iHeps in Hepatogel and H-
387 iHeps in aqueous solution (standard practice) directly into normal livers of immune-
388 compromised mice (NSG™ mice, n=6 each group per time point, 3 time points).
389 NSG™ mice were used to minimize acute cellular rejection from xeno-transplantation.
390 Mice were monitored for human albumin in their serum and then culled for liver
391 histology. Three days after intrahepatic injections, the first group of mice were culled

392 and examined. On post-mortem, It was evident that H-iHeps transplanted in Hepatogel
393 were still present at the injection site, visible as pale-coloured cell masses within the
394 liver. These were more distinct compared to H-iHeps delivered in aqueous solution
395 (0.9% Saline); Fig.6(D).
396
397 Respectively, these macroscopic appearances corresponded to immunofluorescence
398 staining of engrafted cells that were strongly positive for human albumin at the injection
399 sites (cell masses) and not in other regions of the livers; Fig.6(E). Likewise, the number
400 of H-iHeps was significantly higher in liver histology; Fig.6(F). Significantly higher
401 concentrations of human albumin in mice serum were also observed over time and
402 corroborated the histological findings; Fig.6(G). Notably, human albumin remained
403 detectable in mice transplanted with H-iHeps and Hepatogel at Day 6, whereas in mice
404 transplanted with H-iHeps in solution, it was undetectable after the second day,
405 suggesting poor engraftment rates. Nonetheless, beyond 8 days human albumin
406 decreased significantly and was undetectable in both groups. The remaining mice in
407 both groups were culled at 7 days and 2 months after transplantation; no H-iHeps
408 colonies or tumours were seen at the injection sites, demonstrating the clearance of
409 injected H-iHeps by residual innate immunity. In summary, Hepatogel improved the
410 engraftment of H-iHeps compared to standard therapy when injected directly into the
411 liver, however sustained H-iHep proliferation was not observed.
412
413 **DISCUSSION**
414 In this work, we found that a select group of physiologically relevant proteins could be
415 used as biomaterials for 3D hPSC culture. Importantly, we observed that organ-
416 specific hydrogels can produce better end-target phenotypes compared to Matrigel
417 and its derivatives; a generic mouse sarcoma-derived substrate. This was evidenced
418 by significantly higher albumin expression paired with lower fetal liver markers
419 CYP3A7 and AFP in hepatocytes derived from Hepatogel compared to Matrigel. ECM
420 properties vary from organ to organ, in health and disease. Although 2D stem cell
421 culture and organoid technology were established using Matrigel as a central
422 substrate, compositional and mechanical differences to physiological ECM likely
423 contribute to immature phenotypes compared to adult primary cells (45). Importantly,
424 Matrigel derivatives are not approved for clinical use and thus Alphagel is an
425 alternative for 3D hPSC culture and differentiation where hPSCs can be used to derive

426 all cell types in an organ for tissue engineering. In that vein, alternative substrates for
427 hPSC culture, Laminin 521 and vitronectin, are not readily available as pure 3D
428 hydrogels. Laminin 521 has recently been conjugated with silk (Biosilk, Biolamina) to
429 form a generic hydrogel for 3D stem cell and organoid culture (46). However, silk is
430 not native to the human ECM and Biosilk is not licensed for clinical use. Notably, some
431 hPSC differentiation protocols using vitronectin require the dissociation of cells mid-
432 process as well as a change in the substrate (47); this disrupts any early 3D structures
433 that may form in vitro.
434
435 We found that the combination of high Laminin 521 concentrations with low fibrinogen
436 concentrations was a good pairing to create a novel hydrogel for 3D hPSC culture.
437 Physiologically, Laminin 521 and 511 are present in the inner cell mass of the
438 blastocyst and its basement membranes during embryological development (48,49).
439 Its expression remains constant throughout inner cell mass expansion and during
440 differentiation, whereas Laminin 511 expression decreases during differentiation (49).
441 Importantly, through RNAreq of human adult and foetal liver tissue (27), we had
442 established that Laminin 521 is differentially expressed in the maturing fetal liver, along
443 with a small group of ECM proteins that also support stem cell pluripotency to some
444 extent. Notably, Fibrinogen is produced by trophoblasts during early development
445 (50,51), and has the potential for use as an injectable biomaterial being abundantly
446 present in human serum. Cell and protein adhesion is supported by arginine-glycine-
447 aspartate (RGD) binding motifs at positions 96 and 572-574 on the α chains, heparin-
448 binding domains (HBDs) also on the α chains, and a carboxy-terminal peptide
449 (HHLGGAKQAGDV) at position 400-11 on the γ chains (52,53). Likewise, multiple
450 binding sites on the α chains (RGD and HBD) and β chains (mainly RGD) in laminins
451 facilitate cell and protein adhesion (54,55). Importantly, human fibrin is widely used in
452 clinical practice (56), and clinical-grade laminins are commercially available
453 (Biolamina), making the clinical translation of fibrin-laminin hydrogels easily feasible.
454
455 Nonetheless, there are conflicting data on the effects of fibrin hydrogels on stem cell
456 culture. Gandhi et al (57) reported that fibrin gels (30 mg/ml) could be used for iPSC
457 culture. Notably, fibrin concentration is directly proportional to the stiffness of fibrin
458 matrices (58). Our FLGs were finetuned to a Young's modulus of ~ 250-400 Pa to
459 mimic the stiffness of embryological liver (59,60) and the 10 mg/ml fibrin-only gels that

460 we tested had a Young's modulus of ~ 2 kPa. In our experience, high concentrations
461 of fibrin (≥ 4 mg/ml) promoted spontaneous differentiation across 3 hPSC cell lines (2
462 ESC cell lines and 1 iPSC cell line) and this was augmented by the type of stem cell
463 maintenance media used (Supplementary Figure 4). This was evidenced by the low
464 differentiation efficiency and sub-optimal end-target cell phenotypes in fibrin-only
465 hydrogels (e.g. our hepatic differentiation results in Fig.4). and independent studies
466 that showed compliant substrates maintain self-renewal of ESCs by downregulating
467 cell-matrix tractions whilst stiffer substrates promote spontaneous differentiation with
468 downregulation of OCT3/4 expression (61,62). Interestingly, Liu et al (62)
469 demonstrated that compliant fibrin-only gels (1 mg/ml, ~ 100 Pa) promoted the
470 selection and growth of tumour cells that express stem cell markers CD133, Nestin,
471 BMI-1, C-kit but not stem cell markers OCT3 and NANOG. In our study, the addition
472 of Laminin 521 to low-concentration fibrin matrices preserved high OCT4 and NANOG
473 expression in hPSCs over prolonged culture (2-3 months), and similarly fibrin-only
474 hydrogels resulted in absent OCT3 and NANOG expression. Furthermore, no tumour
475 growth was observed after H-iHeps were transplanted into the NSG^{TM} mice. In that
476 vein, the mild local inflammation in the immunocompetent Black 6 mice in our
477 biocompatibility experiments was likely a combination of iatrogenic injury (given similar
478 reactions with saline injections) and the implantation of xenogeneic biomaterials
479 (human ECM proteins). Nonetheless, the mild degree of inflammation and its complete
480 resolution by 6 weeks indicates good biocompatibility that would likely be tolerated
481 well in human studies.
482
483 Since the benefits of fibrin-only matrices are limited in hPSC culture, several groups
484 have recently attempted to create ECM-enriched fibrin hydrogels for regenerative
485 medicine and cell therapy. Laminin 111 enriched fibrin matrices, loaded with (32,63)
486 and without (64,65) cells were used to promote musculoskeletal regeneration after
487 injury. Interestingly, Broguiere et al (22) attempted to mimic Matrigel by enriching fibrin
488 gels with laminin 111 and collagen IV; they then demonstrated it could support the
489 growth of adult stem cells (ASCs) through the propagation of cystic gastrointestinal
490 organoids (intestinal, pancreatic and hepatic organoids). In our experiments, we found
491 that Laminin 111 could maintain hPSC pluripotency (Supplementary Figure 2);
492 however, over limited passages. hPSCs cultured on Laminin 111 were observed to
493 change morphology and form colonies of spontaneously differentiated cells within 1-2

494 weeks (Supplementary Figure 13). Independently, several groups have also
495 concluded that Laminin 111 triggers the spontaneous differentiation of hPSCs; likely
496 through the α1 chain and β1 chain binding to the α3β1-integrin receptor (24–26).
497 Therefore, hydrogels highly enriched with Laminin 111 may be used for ASCs but
498 these are likely to cause phenotypic instability with hPSCs. In our experiments,
499 differentiation efficiency varied between hPSC cell lines, however, these were similar
500 in the reported literature (66–68).
501
502 The organization and polarization of tissues are important to tissue function. In
503 particular, this has been a defining feature previously optimized in neural organoid
504 protocols (69). While these methods typically rely on embedding early aggregates in
505 Matrigel, we show that Alphagel has similar properties, allowing the spontaneous
506 development of organized neural tissue with enlarged apical lumens. Besides
507 consistency, a major advantage of the Alphagel system is that it allows simultaneous
508 differentiation and structural organization without the need for further physical
509 manipulations or tedious time-consuming steps, and thus could be useful to explore
510 as a substrate for brain organoid generation. Similarly, we show the platform is useful
511 in generating 3D cardiac tissue without the need for substrate changes mid-
512 differentiation, thus holding promise in developing injectable regenerative therapies
513 for cardiac disease or ex vivo cardiac tissue engineering.

514 Finally, we demonstrated that Hepatogel improves the engraftment efficiency of H-
515 iHeps in murine livers, highlighting its potential for use as cell therapy for liver disease.
516 At present, human hepatocytes are commonly delivered in solution via injections either
517 directly into the liver or at various vascular sites that feed directly into the liver for cell
518 therapy (70). However, in these approaches, engraftment rates are poor (70,71).
519 Transplanted hepatocytes commonly occupy microvascular spaces, and the resulting
520 ischaemic injury triggers vascular and immune responses within the local niche, which
521 usually has a deleterious effect on the transplanted cells (71). This limits cell
522 engraftment, treatment efficacy and the broader use of cell therapy in liver disease.
523 Other methods of cell delivery involve the injection of cells encapsulated with
524 degradation-resistant matrices such as alginate into the abdomen (72). This is often a
525 temporising measure to bridge patients with liver failure to liver transplantation; in this
526 situation, the encapsulation limits cell engraftment and repopulation. Therefore, we

527 evaluated if biomaterials (Hepatogel) could improve the engraftment rates of
528 transplanted iHeps by replacing the hostile environment with a “regenerative” liver
529 niche. To that end, we show that H-iHeps transplanted into mice liver engrafted better
530 with Hepatogel than H-iHeps in aqueous solution. This was evidenced by the post-
531 mortem findings, higher H-iHep cell counts, and the level of human albumin in mice
532 serum after transplantation; Fig.6(F) to Fig.6(G). However, although Hepatogel
533 improved engraftment, H-iHeps did not proliferate to replace native hepatocytes in the
534 host liver beyond one to two weeks. This may have been caused by the
535 immunogenicity of hPSC cells (73), limitations of current iHep technology (74), or
536 immunological responses in the recipient mice; NSG™ mice have preserved
537 neutrophils and monocyte function. Limited repopulation of transplanted iHeps
538 remains a universal challenge, and our long-term observations are similar to others
539 reported in the literature (71). Nonetheless, as biotechnology advances, the derivation
540 of high-quality non-immunogenic lab-derived hepatocytes will improve, and clinically
541 applicable hydrogels will serve as useful adjuncts in hepatocyte derivation and cell
542 therapy by improving cell delivery, engraftment, and treatment efficacy (20).
543

544 **CONCLUSION**

545 We have shown proof-of-concept that bioengineered organ-specific hydrogels can
546 improve the phenotypes of hPSC-derived end-target cells compared to generic
547 hydrogels. Our fully defined and liver-specific hydrogel (Hepatogel) increased gene
548 expression and metabolic function in induced hepatocytes compared to Matrigel.
549 Being biodegradable, injectable, and composed of clinical-grade biomaterials,
550 Hepatogel may serve as a useful clinical adjunct to improve hepatocyte engraftment
551 for cell therapy.
552

553 **MATERIALS AND METHODS**

554 *Protein Screening*

555 Protein screening was performed using the Opera Phenix High-Content High-
556 Throughput (HCHT) screening system (PerkinElmer, USA). Briefly, the MFI of OCT4,
557 NANOG, and SOX2, were measured in hPSCs (positive control) cultured on Geltrex
558 (Thermofisher, #A1413302) and human fibroblasts (negative control) cultured on
559 uncoated plates. Optimised antibody concentrations are listed below. Nuclear
560 measurements were measured using DAPI. Differential characteristics between the

561 two populations were used to identify thresholds for machine learning. A screening
562 pipeline was created using Harmony High-Content Imaging and Analysis software
563 (Perkin Elmer, USA) and validated for accuracy as reported. hPSCs were then plated
564 on 96-well tissue culture-treated plates (Greiner Cellstar, #M0812) coated with single
565 substrates at 4 different concentrations. The measure of pluripotency within a stem
566 cell population was then defined as the "Stemness Index" (SI), which was calculated
567 by:

568

569 $$\textit{Stemness Index (SI)} = \frac{\textit{Total number of Stem Cells Identified}}{\textit{Total number of Cells In Population}}$$

570

571 The maximum values of SI are 0 and 1, and the equation was incorporated into the
572 pipeline. This enabled the automated calculation of results and identification of
573 proteins that maintained stem cell pluripotency. Positive hits were checked using
574 brightfield microscopy.

575

576 *2D cell culture*

577 hPSCs were maintained on Geltrex-coated plates in feeder-free mTeSR-1™ and
578 mTeSR Plus™ media (Stemcell Technologies #85850 and #100-0276) using an
579 established protocol (75). Geltrex was substituted for other substrates during protein
580 screening. During maintenance, cells were split at 70-80% confluence using Accutase
581 (Millipore, #SCR005), washed with DMEM/F12 (Life Technologies, #11330032) and
582 re-seeded onto Geltrex-coated 6-well plates (Greiner, #657160) at a ratio of 1:6 to 1:8.
583 1mM Y27632 ROCK inhibitor (Stratech Scientific, #S1049-SEL-2mg) was used to
584 increase cell attachment. Media was supplemented with penicillin and streptomycin
585 (Millipore, #TMS-AB2-C). For screening experiments, human ESCs (KCL033) and
586 human iPSCs (RMA and BOB cell lines) were used. These were gifted by Dr Tamir
587 Rashid (King's College London). For other experiments, 2 ESC cell lines (H1 and H9,
588 WiCell #WA01 and #WA09 respectively) and 1 episomal iPSC cell line (ThermoFisher,
589 #A18945) were used. Cell viability in 2D and 3D experiments was assessed using
590 Trypan Blue (Sigma, #15250061).

591

592 Human dermal fibroblasts were available in-house (Sigma, #106-05a). Depending on
593 experiments, these were cultured either on uncoated tissue culture flasks (Corning,
594 #CLS3275) or Geltrex-coated 6-well plates. Fibroblasts were maintained in
595 DMEM/F12 media (Life Technologies, #11330032), 10% foetal bovine serum (Sigma,
596 #A9418), and 1% penicillin and streptomycin (Millipore, #TMS-AB2-C). Fibroblasts
597 were passaged using Trypsin (ThermoFisher, #11538876).
598
599 Primary human hepatocytes from 3 different non-diseased donors were obtained
600 commercially (Lonza, #HUCPI). These were quality-controlled, characterised and
601 came from three different lots; Lot no. HUM182701, HUM182641, and HUM191381.
602 Cells were thawed, plated on collagen-1 coated plates, and recovered for at least 24
603 hr in Hepatocyte Culture Media™ (HCM) including the complete HCM bullet kit (Lonza,
604 #CC-3198) according to the supplier's protocol. Experiments commenced after 24 –
605 48 hr of cell recovery.
606
607 *3D cell culture*
608 hPSCs were cultured in 3D domes of Matrigel, fibrin-only gels, or FLGs plated on
609 hydrophobic non-tissue culture-treated hydrophobic plates under normoxic conditions
610 at 37 ^{o}C. 50 µl domes were used for 24-well plates (Sarstedt, #83.3922.500) or 25 µl
611 domes for 96-well plates (Ibidi, #89621). H1, H9 and episomal cell lines were used for
612 these experiments. Feeder-free mTeSR-1™ and mTeSR Plus™ media (Stemcell
613 Technologies #85850 and #100-0276) were used for routine stem cell maintenance.
614 hPSCs designated for animal experiments were maintained in xeno-free TeSR™ 2
615 media (Stemcell Technologies, #05860). Cells were split every 5-6 days using TrypLE
616 Express (Gibco, #12604013). Each dome required 20-25 min in TrypLE Express with
617 manual pipetting for successful dissociation. Domes were then re-loaded with 12,500
618 to 225,00 cells depending on experiments.
619
620 For experiments investigating the effect of stem cell culture media on hPSC
621 pluripotency in Alphagel, TeSR-E8™ culture media (Stemcell Technologies, #05990),
622 E8™ culture medium (ThermoFisher, #A1517001), and TeSR-E8TM culture medium
623 (Stemcell Technologies, #05990) were used in addition to those described above. All
624 culture media were supplemented with 1% penicillin and streptomycin (Millipore,

625 #TMS-AB2-C). Media were refreshed on alternate days. EBs formed after three to four
626 days in FLGs and Matrigel.
627
628 *3D cardiac differentiation*
629 hPSCs designated for cardiac differentiation were transitioned to E8^{TM} culture medium
630 (ThermoFisher, #A1517001) supplemented with 2.25 ng/ml of Fibroblast Growth
631 Factor-2 (FGF-2: Qkine, #Qk053), and 1.74 ng/ml of Transforming Growth Factor Beta
632 (TGF-b: Bio-techne, #7754-BH). This media is primed for cardiac differentiation as
633 previously described (76). When hESC colonies reached the desired number and size,
634 cardiac differentiation was initiated using a previously established protocol (77).
635 Briefly, mesodermal specification was initiated by replacing the FGF-2 and TGF-b
636 enriched E8 maintenance media with CDM-BSA (Sanjay Sinha Lab, University of
637 Cambridge) containing 20 ng/ml of FGF-2/ml, 10 μM of 2-(4-Morpholinyl)-8-phenyl-4
638 H-1-benzopyran-4-one (Ly294002: Promega, #V120A), 50 ng/ml of Activin A
639 (Stemcell Technologies, #78132.2), and 10 ng/ml of Bone Morphogenic Protein-4
640 (BMP-4: RnD system, #314-BP-050). After 42 hr (Day 1.5), this was replaced with
641 CDM-BSA containing 8 ng/ml of FGF-2, 10 ng/ml of BMP-4, 1μM of retinoic acid
642 (Sigma, #R2625) and Wnt/β-catenin signalling inhibitor endo-IWR1 (R&D systems,
643 #3532). Media was refreshed after 48 hr (Day 3.5). After another 48 hr (Day 5.5), the
644 media was replaced with CDM-BSA containing 8 ng/ml of FGF-2 and 10 ng/ml of BMP-
645 4. Standard CDM-BSA media was then refreshed every 48 hr (Day 7.5 onwards).
646
647 *3D neuronal differentiation*
648 hPSCs designated for neuronal differentiation were transitioned into Stem Flex media
649 (ThermoFisher, # A3349401) with the addition of 10μM Y-27632 (Tocris, #1254)
650 before initiating differentiation. Media was refreshed daily. When EBs were of sufficient
651 number and size in Alphagel, neuronal differentiation was performed using an
652 established protocol (78). Briefly, after four days of expansion in Alphagel with Stem
653 Flex media, the media was switched to N2B27 media (in-house) supplemented with 5
654 μM SB-431542 (Tocris, #1614), 200 nM LDN-193189 (Miltenyi, #130-103-925), and 2
655 μM XAV-939 (Tocris, #3748). Media with these factors was refreshed daily for ten
656 days. After this, cells were maintained in N2B27 media only for a further six days.
657
658 *3D hepatic differentiation*

659 Hepatocyte differentiation was performed using a previously established protocol (75).
660 Briefly, hPSCs were cultured in RMPI (ThermoFisher, #22400089) supplemented with
661 2% B27 minus insulin (ThermoFisher, #A1895601), 100 ng/ml of Activin A, 20 ng/ml
662 of FGF-2 (ThermoFisher, #PHG0023) and 10 ng/ml of Bone Morphogenic Protein-4
663 (BMP-4: R&D system, #314-BP-050) on differentiation days 1 — 2 to initiate
664 differentiation. From differentiation days 3 — 5, the media was replaced with RMPI
665 supplemented with 2% B27 minus insulin and 100 ng/ml Activin A only. Hepatic
666 endoderm specification was initiated on differentiation days 6 — 10 using RMPI
667 supplemented with 2% B27 and insulin (ThermoFisher, #17504044), 10 ng/ml FGF-2,
668 and 20 ng/ml BMP-4, followed by RMPI with 2% B27, insulin, and 20 ng/ml hepatocyte
669 growth factor (HGF: Peprotech, #100-39-250) on differentiation days 11 — 15.
670 Maturation of hepatic endoderm was initiated on differentiation days 16 — 21 using
671 complete HCM media supplemented with 10 ng/ml Oncostatin M (OSM: R&D systems,
672 # 8475-OM-050), 20 ng/ml HGF and 0.1 μM Dexamethasone (ThermoFisher,
673 #A17590.06).
674
675 *Synthesis of fibrin hydrogels*
676 Human fibrinogen from non-diseased donors (Merck Millipore, #341576-1GM) was
677 reconstituted in sterile 0.9% saline to a stock concentration of 67 mg/ml. Human
678 thrombin (Sigma, #T6884-100UN) was reconstituted in sterile 0.9% saline
679 supplemented with human serum albumin (0.1% w/v) giving a stock concentration of
680 50 U/ml. DMEM/F12 was then added to various volumes of fibrinogen and thrombin
681 to achieve the desired final fibrinogen concentration of the fibrin gels. Final fibrinogen
682 concentrations in the hydrogels that we tested ranged from 1 mg/ml to 10 mg/ml. The
683 final concentration of thrombin in these hydrogels was maintained at 1 U/ml. For cell
684 experiments, hPSCs were loaded into the DMEM/F12 compartment.
685
686 *Synthesis of Alphagel and Hepatogel*
687 Alphagel and Hepatogel were synthesised using similar methods of fibrin-laminin
688 enrichment previously reported (22,32) with minor adjustments. Briefly, for acellular
689 Alphagel domes, human recombinant laminin 521 (Biolamina, #CT521-0501/LN521-
690 05), human fibrinogen and DMEM/F12 were incubated in sterile Eppendorf (Elkay Lab,
691 #MICR-050) at 37 ^{o}C for 15 min. The mixture was then mixed and left to incubate for
692 a further 15 min. Lastly, thrombin diluted in DMEM/F12 at room temperature was

693 added to the mixture for gelation. 50 µl domes of the final mixture were then plated on
694 24-well flat bottom hydrophobic plates (Sarstedt, #83.3922.500) using wide bore
695 pipette tips (Starlab UK, #I1011-8000). The final composition of Alphagel contained a
696 50:50 v/v mixture of Laminin 521, 2.5 mg/ml fibrinogen and 1 U/ml thrombin. For
697 Hepatogel, Laminin 411 (Biolamina, #LN411) and Laminin 111 (Biolamina, #LN111)
698 were first purified using Amicon Ultra-0.5 centrifugal filter units (Merck Millipore,
699 UFC5003) and reconstituted in sterile PBS. Then, Laminin 521, 411, and 111 were
700 mixed in the respective ratio of 5:1:2. For cell experiments, hPSCs were loaded in the
701 laminin(s)-DMEM/F12-fibrinogen compartment and incubated as described above.
702 Lastly, the thrombin-DMEM/12 compartment was added for polymerisation. The cell-
703 laden mixture was then seeded at 50 µl per dome in 24-well plates and inverted to
704 allow the cells to remain suspended in 3D. These plates were kept inverted for a further
705 30 min to allow to gelation complete fully. Thereafter, plates were turned over and 1
706 ml of media was added to each well. Media was refreshed at a frequency determined
707 by experiments.
708
709 *Scanning Electron Microscopy (SEM)*
710 Fibrin-only hydrogels and FLGs samples for SEM were prepared following a previously
711 published protocol (79). Briefly, fibrin-only and FLGs were mounted and gelled in 444
712 ferritic stainless-steel scaffolds (Nikko Techno Ltd., Japan) for mechanical support. An
713 hour after gelation, samples were fixed in 10% formalin (VWR International,
714 #11699455) and left in a fume hood overnight. The following day, samples were
715 washed three times with PBS and then dehydrated in increasing concentrations of
716 ethanol-de-ionised (DI) water mixtures; 30, 50, 70, 80, 90, 95 and 100% ethanol. The
717 final step with 100% ethanol was repeated twice. Samples were submerged for 30 min
718 in each ethanol-DI mixture. For dehydration, the samples were immersed in increasing
719 concentrations of hexamethyldisilazane (HMDS)-ethanol mixtures in a fume hood;
720 33.3, 66.6 and 100% HMDS (Sigma, #440191) respectively. Samples were immersed
721 in each HMDS-ethanol mixture for 40 min. The final step involving 100% HMDS was
722 repeated twice, and then samples were left submerged in 100% HMDS overnight in a
723 fume hood until completely dry the following day. Dried samples were gold plated
724 before imaging with Evo LS 15 (Zeiss, Germany) scanning electron microscope.
725
726 *Immunofluorescence (IF) staining*

727 For 2D protein screening experiments, culture media was aspirated, and cells were
728 washed twice with phosphate buffer saline (PBS; Sigma, #806552) using volumes of
729 100 µl per well for 96-well plates. Fixation was performed using 4% paraformaldehyde
730 (PFA, Insight Biotechnology, #sc-281692) for 20 min at 4 ^{o}C followed by two further
731 PBS washes. 50 µl of blocking solution containing 3% donkey serum (Sigma, #D9663-
732 10ML), 0.1% Triton-X (Sigma, #X100-500ML), 1% BSA (Sigma, #12657), and 95.9%
733 PBS was then added to each well. The plate was left for 30 min at room temperature
734 for permeabilization, and blocking, then aspirated for the addition of the primary
735 antibodies without washing. The list of primary antibodies is listed in Table 1. After two
736 hr at room temperature, the primary antibodies were aspirated, and cells were washed
737 twice with 100 µl/well PBS in each wash. 50 µl/well of secondary antibodies were then
738 added and samples were left to incubate at room temperature in the dark for 2 hr. The
739 list of secondary antibodies is listed in Table 2. After 2 hr, secondary antibodies were
740 aspirated, and cells were washed twice with PBS (100 µl/well) followed by the addition
741 of DAPI solution (NucBlue^{TM} Fixed, Life Technologies #R37606). Imaging was then
742 performed within 24 hr.
743
744 For 3D cardiac and hepatic experiments, cell-laden hydrogel domes first underwent
745 two fifteen-minute washes with PBS (1 ml/well for a 24-well place). Samples were then
746 fixed for 60 min at 4 ^{o}C with 4% paraformaldehyde (1 ml/well) followed by three 15 min
747 washes with PBS (1ml/well). Subsequently, cells were permeabilized and blocked in
748 1% (w/v) bovine serum (Sigma, #A9418), 3% donkey serum (Sigma, #D9663), and
749 0.1% Triton X-100 (Sigma, #X100) in sterile PBS for one hour at room temperature.
750 The blocking solution was then aspirated, and primary antibodies (1ml/well) were
751 added without any washing. Samples were left overnight at 4 ^{o}C to incubate. The
752 following day, primary antibodies were aspirated, and samples underwent two fifteen-
753 minute PBS washes. Next, secondary antibodies were added, and samples were left
754 in the dark at room temperature to incubate for ≥3 hr. Thereafter, the DAPI solution
755 was added and images were acquired at least 30 min after the addition of the DAPI
756 solution. For 3D neural experiments, hydrogels were fixed in 4% PFA for 45 min at
757 room temperature then transferred into a 30% w/v sucrose solution (Sigma Aldrich,
758 #S0389) and left for 24 hr. Sucrose-saturated samples were subsequently placed in
759 OCT (ThermoFisher, #23-730-571) and stored at -20 ^{o}C. These frozen blocks were
760 then cut into 12 µm sections and mounted on coated slides (ThermoFisher,

761 #J1800AMNZ). Sections were then blocked and permeabilised in a 0.3% Triton-X
762 solution containing 10% normal goat serum at room temperature for an hour. Primary
763 antibodies diluted in 0.1% Triton-X containing 5% normal goat serum were then added
764 and incubated overnight at 4 °C. The following day, sections were washed with PBS
765 and secondary antibodies were added and left for an hour at room temperature. Lastly,
766 samples were incubated in DAPI solution for 15 min and then mounted using
767 FluorSave (VWR, #345789).
768
769
770
771 Table 1: List of primary antibodies.
772

Primary Antibodies (species raised in)	***Vendor***	***Catalogue no.***	***Dilution factor***
OCT4 (rabbit)	ThermoFisher	710788	1:250
NANOG (rabbit)	Abcam	ab109250	1:100
SOX2 (rabbit)	ThermoFisher	PA1-094	1:100
SOX2 (goat)	RnD Systems	AF2018	10 µg/ml
Albumin (goat)	Bethyl	A80-129A	1:100
CD147 (mouse)	Abcam	Ab666	1:100
HNF1A (rabbit)	Cell Signalling	D7Z2Q	1:400
HNF4A (rabbit)	ThermoFisher	MA5-14891	1:2000
Cyp2A6 (chicken)	University of Eastern Finland	Collaborator	1:200
E-cadherin (mouse)	Santa Cruz	SC-31021	1:100
Troponin-T (goat)	Abcam	ab64623	1:100
Smooth Muscle α-Actin (mouse)	Dako	M0851	1:100
Nestin (mouse)	Sigma	N5413-100UG	1:500
B-catenin (rabbit)	ThermoFisher	14-2567-82	1:250

773
774
775 Table 2: List of secondary antibodies.
776

Secondary Antibodies	*Vendor*	*Catalogue no.*
AlexaFluor 488 donkey anti-goat	ThermoFisher	A11055
AlexaFluor 488 donkey anti-rabbit	Abcam	ab150073
AlexaFlour 488 donkey anti-rabbit	ThermoFisher	A21206
AlexaFluor 564 donkey anti-mouse	ThermoFisher	A10037
AlexaFluor 647 donkey anti-rabbit	Abcam	ab150075
AlexaFluor 647 donkey anti-mouse	ThermoFisher	A32795
AlexaFluor 647 donkey anti-mouse	ThermoFisher	A31571

For IF staining of tissue sections, glass slides with paraffin-embedded sections were rehydrated in xylene (5 min x3), then transferred to reducing concentrations of ethanol (100% for 5 min x2, 90% for 2 min, and 70% for 2 min). Thereafter, slides were washed in distilled water for 5 min and transferred to pH 6.0 antigen retrieval buffer and heated to 121 °C for 15 min. After cooling, the slides were re-washed with distilled water. A hydrophobic pen was used to mark the area of interest. Then, TrueBlack® (Biotium, #23007) dissolved in 70% ethanol (1X) was added to the samples for 30 sec to reduce autofluorescence. Subsequently, slides were rinsed with distilled water and blocking solution, as described above, was added and the samples were left for 30 min at room temperature. After 30 min, the blocking solution was discarded without washing the samples and goat anti-human albumin primary antibody dissolved in sterile PBS to a final concentration of 1:100 ((as described above) was added to the samples. Slides were then left to incubate at 4 °C overnight. The following day, the slides were washed with distilled water, and then 1:200 Alexa Fluor 647 donkey anti-goat secondary antibody (as above) was added. The slides were left for one hour to incubate in the dark at room temperature and then washed again before adding Fluoroshield™ mounting media containing DAPI (Sigma, #F6057). Lastly, coverslips were placed and sealed with nail polish.

Imaging

2D IF and brightfield images of hPSCs were acquired using the Opera Phenix HCHT screening system (PerkinElmer, USA). Optimal acquisition settings were determined

801 as 100 ms exposure time and 90% excitation strength; these were kept constant
802 during screening. 3D images of cardiac and hepatic cells and tissue were captured
803 using an LSM710 (Zeiss, Germany) laser scanning confocal microscope at x10 and
804 x20 objectives with corresponding filters. Bright-field images were acquired using an
805 Axio-Obsorber.Z1 (Zeiss, Germany) fluorescence microscope. Images of CDFDA
806 uptake and excretion in iHeps were acquired using an SP-DM8 (Leica, Germany)
807 microscope. 3D images of neuronal cells were acquired using a DM 6000 B (Leica,
808 Germany) microscope.
809
810 *Young's modulus measurements*
811 Fibrin-only and FLGs were examined under compression using a customised "see-
812 saw" method that was previously described (80) and loads were applied by pumping
813 liquid via a syringe pump. This method minimises sample strain during measurements
814 - excessive straining occurs easily with such highly compliant materials and can
815 produce misleading results. Briefly, two arms of a see-saw were first balanced before
816 counterweights were added onto the free-extending arm to match the height of the
817 loading platen with the sample height. Next, the load was ramped up at a constant rate
818 of 10^{-3} N s^{-1} by pumping liquid, via a PHD ULTRA syringe pump (Harvard Apparatus,
819 USA), into a container fixed on top of the loading platen. The resulting displacement
820 was measured using a biaxial laser micrometre (resolution of ±3 μm, Keyence, #TM-
821 040). Nominal stresses (σ) and strains (ε) were plotted, and a line was least-square
822 fitted to the data points. From the tangent slope of the stress-strain curves, the
823 through-thickness Young's modulus was calculated (n=5 in each group).
824
825 *Gene expression analyses by quantitative polymerase chain reaction (qPCR)*
826 Ribonucleic acid (RNA) was extracted using TriZOL™ (ThermoFisher, #15596026)
827 and purified using the Direct-zol RNA Miniprep Kit (Zymo Research, #R2050-R2053).
828 cDNA was made using Superscript Reverse Transcriptase IV (ThermoFisher,
829 #18090010) following the manufacturer's protocol. Quantitative PCR was run on
830 Quantstudio 5 (ThermoFisher, #A34322I) using the KAPA SYBR FAST qPCR kit
831 (Roche, #KK4601). Data were analysed using the 2^(ΔΔCt) method. Sequences of
832 the primer pairs are listed in Table 3.
833
834 Table 5.3: Sequences for forward and reverse primers used.

Target gene	*Forward primer sequence*	*Reverse primer sequence*
ABCC2	TTCGTTCCAGACGCAGTCCAGG	CCAGGAGCCATAGGTAGCCCAA
APOB	TGTTAGGACACCAGCCCTCCA	GCCCGAAGGCTGAAATGGTCT
AFP	AACTATTGGCCTGTGGCGAGG	TGAAGCATGGCCTCCTGTTGG
BAAT	TGTGCCTCAACGACCCACGAT	GGGGGAGACATTCCGCCATGAA
CEBPA	AAGTCGGTGGACAAGAACAGCAA	TTGTCACTGGTCAGCTCCAGCA
CYP27A1	GCTGTTCGTTCAAGGCTATGCCC	ACTGGGTACTTGCCCTCTTGCC
CYP3A4	TGTGCCTGAGAACACCAGAG	GTGGTGGAAATAGTCCCGTG
CYP3A5	ACAAGACCCCTTTGTGGAGAGC	TTGTTTGTCGTTGAGGCGACTT
CYP3A7	TGGACCCAGAAACTGCATTGGC	ATCAGGCTCCACTTACGGTCTCA
CK7	AAGCAGGATATGGCACGGCAG	CACTCCATCTCCAGCCAACCG
CK19	GGCGATGTGCGAGCTGATAGT	CGGTAGGTGGCAATCTCCTGC
FOXA1	CCTTCAACCACCCGTTCTCCA	CGGGCAACGTAGAGCCGTAAG
FOXA2	GCCTACGAACAGGTGATGCACTA	CAGGCCCGTTTTGTTCGTGAC
GATA6	AGCACCAATCCCGAGAACAGC	GTCGCACGGAGGACGTGACTT
GATA4	TCCATCCACCCTGTCCTCTCG	GCTTGGAGCTGGTCTGTGGAG
G6PC	TACAGCAACACTTCCGTGCCCC	GCACAGCCCAGAATCCCAACCA
GGT	ACAACCAGCTTCTGCCCAACG	GACGCGATCTGGGTGTGATGG
HNF4A	GAGATGCTGCTGGGAGGGTCC	GGGTCTCAGGGGTGGACATCT
LGR5	CCTGCTTGATGGCTGGCTGAT	CACTGCTGCGATGACCCCAAT
PDK4	TACAGCAACACTTCCGTGCCCC	GCACAGCCCAGAATCCCAACCA
SOX9	CAACAGATCGCCTACAGCCCC	CGTACTGTGAGCGGGTGATGG
TAT	TGGAAACCTGCCTACAGACC	TAGCTTCTAGGGGTGCCTCA
TF	CCGATGGTCCCAGTGTTGCTT	AACTCTGCCACCACAGGCTTC
TBX3	GGGACACTGGAAATGGCCGAA	GGAGAAGAAGCCTGGGCGAAG
MUC2	GCTGACGAGTGGTTGGTGAATG	GATGAGGTGGCAGACAGGAGAC

Enzyme-linked immunosorbent assays (ELISA)

Laminin concentrations in supernatants were measured using a laminin ELISA kit (Insight Biotechnology, #Boster Pikokine™ EK0434). Acellular FLGs and fibrin gels were synthesized, and sterile DMEM/F12 media was added 30 min after gelation. Media was collected the next day (Day 1) and then every other day for two weeks. Supernatants were stored at -20 °C until they were analysed alongside stock concentrations of laminin for comparison using the Laminin ELISA kit as per the manufacturer's instructions. Sample absorbance readings were then taken using a FLUOstar® Omega plate reader (BMG Labtech Ltd, UK) at 450 nm. The residual amount of laminin in FLGs was estimated by the following equation:

$$1 - \frac{Total\ Laminin\ 521\ in\ supernatant\ after\ hydrogel\ gelation\ (weight)}{Measured\ Laminin\ 521\ in\ stock\ solution\ added\ to\ the\ hydrogel\ (weight)}$$

849

850 Albumin concentrations in supernatants were measured using a human albumin
851 ELISA quantification kit (Bethyl Lab, #E80-129). Sample absorbance was measured
852 with a Synergy HTX microplate reader (BioTek, USA). Supernatants from PHH
853 hepatocytes were collected 24 hr after the completion of cell recovery. Supernatants
854 from iHeps were collected 2 days after (Day 22) the end of the differentiation protocol
855 (Day 20); media was refreshed every other day as per differential protocol).
856
857 APOB secretion in the supernatant was quantified using the human APOB ELISA
858 quantification kit (Mabtech, # 3715-1H-6) according to product literature. Sample
859 absorbance was measured with an Infinite M1000 PRO microplate reader (Tecan,
860 Switzerland). Supernatants from iHeps were collected 2 days after (Day 22) the end
861 of the differentiation protocol (Day 20); media was refreshed every other day as per
862 differential protocol).
863
864 *Cytochrome 3A4 (CYP3A4) assay*
865 CYP3A4 activity was measured using the P450-Glo^{TM} CYP3A4 Assay kit (Promega,
866 #V9001) as per the manufacturer's protocol. Fluorescence in samples was measured
867 using the Synergy HTX microplate reader. PHH after 24 hr of cell recovery and Day
868 22 iHeps were used.
869
870 *Low-density Lipoprotein (LDL) uptake cell-based assay*
871 LDL uptake was demonstrated using a cell-based kit (Cayman chem, #10011125)
872 following the manufacturer's protocol. iHeps were incubated for 12 hr, then the HCM
873 media was replaced with PBS. Images were then acquired immediately. Day 22 iHeps
874 and hPSCs (negative control) were used.
875
876 *5-(and-6)-Carboxy-2',7'-Dichlorofluorescein Diacetate (6-CDF)*
877 6-CDF was used to demonstrate hepatocyte function following a protocol previously
878 described (39). 3D iHeps (Day 22) were incubated for 2 hrs with HCM media
879 containing 1 µmol/L of 6-CDF (Thermofisher, #C-369). Samples were then washed
880 with PBS for 15 min before staining with Hoescht in HCM.
881

882 Gamma-glutamyl Transfer (GGT) assay
883 GGT activity was determined by a fluorometric GGT assay kit (Abcam, #ab241030) as
884 per product literature. Fluorescence in samples was measured with the Infinite M1000
885 PRO microplate reader. PHH after 24 hr of cell recovery and Day 22 iHeps were used.
886 PHH after 24 hr of cell recovery and Day 22 iHeps were used.
887
888 *Animal experimentation*
889 Biocompatibility studies were performed in immunocompetent general-purpose
890 C57BL/6 ("Black 6") mice obtained from InVivos (www.invivos.com.sg). Only healthy,
891 normal strain male mice between two to three months old (~ 30 g to 35 g) were used.
892 100% croton oil (Merck, #C6719-10G) was emulsified in corn oil to a final
893 concentration of 1.0% *v/v, referred to herein as "croton oil".* Croton oil was used as a
894 positive control because it is a well-known skin allergen that is commonly used to study
895 inflammation in murine models (81). 200 µl of croton oil (n=9), Alphagel (n=9), fibrin-
896 only gel (n=9), and 0.9% saline (n=9) was injected subcutaneously using 18G
897 hypodermic needles and 1 ml low dead volume syringes into the flanks or scruffed
898 backs of Black 6 mice with aseptic techniques. These volumes were within
899 internationally recommended limits for subcutaneous murine injections (American
900 Association for Laboratory Animal Science). Three mice from each group were culled
901 at 1 week, 2 weeks, and 6 weeks post-injection. Mice were culled by cervical
902 dislocation under general anaesthesia with isofluorane. Injection sites were excised
903 and fixed in 10% formalin for 24 hr then transferred into 70% ethanol. Tissues were
904 then embedded in liquid paraffin, sectioned by microtome, and placed on glass slides.
905 Slides were stained for hematoxylin and eosin (H&E) to allow for evaluation for signs
906 of inflammation, then imaged with the TissueFAXS i-plus system (TissueGnostics,
907 Vienna, Austria).
908
909 Both male and female mice were used. All mice were between four to five months old
910 and weight ~ 40 g to 50 g. All mice were anaesthetised with isoflurane and had their
911 abdomen shaved pre-operatively. Surgical laparotomies were then performed
912 aseptically to reveal the lower liver margin for injections. For H-iHep transplantations,
913 3 x 10^6 million freshly harvested Day 22 H-iHeps were harvested and re-suspended in
914 75 µl of either Hepatogel (n=9) or sterile 0.9% saline (n=9), then injected under direct
915 vision with a 1 ml low dead volume syringe and 18G hypodermic needle into the inferior

916 margins of the right liver lobe. All mice were given prophylactic antibiotics and
917 analgesia subcutaneously for three days after the operation. 3 mice from each group
918 were culled on Day 3, Day 7-, and 2 months post-hepatocyte transplantation.
919
920 All mice were fed rodent maintenance food (#2918 Teklad Irradiated Global, 18%
921 Protein rodent diet, Envigo, Hackensack, NJ) and kept on bedding from BioCOB.
922 Approval for all animal work was granted by the National University of Singapore
923 Institutional Animal Care and Use Committee (IACUC), protocol number R20-0822.
924
925 *Statistical analyses*
926 Prism 9.3.0 (GraphPad, USA) was used for data analyses and the generation of bar
927 graphs. Data were tested for normal distribution using the Shapiro-Wilk method.
928 Parametric data and their bar charts were presented as mean and standard deviation
929 unless otherwise stated. For comparison between two groups of values, the student's
930 t-test was used to compare means for parametric values; the Chi-squared test or
931 Mann-Whitney U test was used to test for associations in non-parametric values.
932 When more than two groups were compared, one-way analysis of variance (ANOVA)
933 with Tukey correction was performed on parametric data; the Kruskal-Wallis test was
934 used when data were not parametric All tests were two-sided, and the alpha was set
935 at 5%.
936
937
938 **Data availability statement:** The authors confirm that the data supporting the findings
939 of this study are available within the article and/or its supplementary materials.
940
941 **Funding statement:** JO was supported by the University of Cambridge (UoC) WD
942 Armstrong graduate studentship, the UoC Engineering in Clinical Practice grant, the
943 National University of Singapore (NUS) Talent Development grant, and the NUS
944 Postdoctoral Development grant. JZ was supported by Trinity College and the
945 Cambridge Commonwealth, European, and International Trust (UoC). AWJ was

946 supported by an Engineering and Physical Sciences Research Council grant, the
947 Rosetree Trust and the Isaac Newton Trust.

948

949 **Conflict of Interest Disclosure:** The authors have none to declare.

950

951 **Ethics approval statement:** This study did not involve human subjects. The National
952 University of Singapore Institutional Animal Care and Use Committee (IACUC) granted
953 ethical approval for animal research, *protocol number R20-0822.*

954

955 **References**

956 1. Hofer M, Lutolf MP. Engineering organoids. Nat Rev Mater. 2021 May;6(5):402–20.

957 2. Pampaloni F, Reynaud EG, Stelzer EHK. The third dimension bridges the gap between cell culture
958 and live tissue. Nat Rev Mol Cell Biol. 2007 Oct;8(10):839–45.

959 3. Gjorevski N, Nikolaev M, Brown TE, Mitrofanova O, Brandenberg N, DelRio FW, et al. Tissue
960 geometry drives deterministic organoid patterning. Science. 2022 Jan 7;375(6576):eaaw9021.

961 4. Salthouse D, Novakovic K, Hilkens CMU, Ferreira AM. Interplay between biomaterials and the
962 immune system: Challenges and opportunities in regenerative medicine. Acta Biomater. 2023 Jan
963 1;155:1–18.

964 5. Chan SW, Rizwan M, Yim EKF. Emerging Methods for Enhancing Pluripotent Stem Cell Expansion.
965 Front Cell Dev Biol [Internet]. 2020 Feb 14 [cited 2024 Dec 17];8. Available from:
966 https://www.frontiersin.org/journals/cell-and-developmental-
967 biology/articles/10.3389/fcell.2020.00070/full

968 6. Heo JH, Kang D, Seo SJ, Jin Y. Engineering the Extracellular Matrix for Organoid Culture. Int J Stem
969 Cells. 2022 Feb 28;15(1):60–9.

970 7. Aisenbrey EA, Murphy WL. Synthetic alternatives to Matrigel. Nat Rev Mater. 2020 Jul;5(7):539–
971 51.

972 8. Baker M. Stem cells in culture: defining the substrate. Nat Methods. 2011 Apr;8(4):293–7.

973 9. Vukicevic S, Kleinman HK, Luyten FP, Roberts AB, Roche NS, Reddi AH. Identification of multiple
974 active growth factors in basement membrane Matrigel suggests caution in interpretation of
975 cellular activity related to extracellular matrix components. Exp Cell Res. 1992 Sep;202(1):1–8.

976 10. Soofi SS, Last JA, Liliensiek SJ, Nealey PF, Murphy CJ. The elastic modulus of Matrigel as
977 determined by atomic force microscopy. J Struct Biol. 2009 Sep;167(3):216–9.

11. Hughes CS, Postovit LM, Lajoie GA. Matrigel: a complex protein mixture required for optimal growth of cell culture. Proteomics. 2010 May;10(9):1886–90.

12. Passaniti A, Kleinman HK, Martin GR. Matrigel: history/background, uses, and future applications. J Cell Commun Signal. 2022 Dec;16(4):621–6.

13. Liu H, Bockhorn J, Dalton R, Chang YF, Qian D, Zitzow LA, et al. Removal of lactate dehydrogenase-elevating virus from human-in-mouse breast tumor xenografts by cell-sorting. J Virol Methods. 2011 May;173(2):266–70.

14. Segers VFM, Lee RT. Biomaterials to enhance stem cell function in the heart. Circ Res. 2011 Sep 30;109(8):910–22.

15. Farhat W, Hasan A, Lucia L, Becquart F, Ayoub A, Kobeissy F. Hydrogels for Advanced Stem Cell Therapies: A Biomimetic Materials Approach for Enhancing Natural Tissue Function. IEEE Rev Biomed Eng. 2019;12:333–51.

16. Cruz-Acuña R, Quirós M, Huang S, Siuda D, Spence JR, Nusrat A, et al. PEG-4MAL hydrogels for human organoid generation, culture, and in vivo delivery. Nat Protoc. 2018 Sep;13(9):2102–19.

17. Amzad Hossain M, Kumar Roy C, Don Sarkar S, Roy H, Hasan Howlader A, H. Firoz S. Improvement of the strength of poly(acrylic acid) hydrogels by the incorporation of functionally modified nanocrystalline Cellulose. Mater Adv. 2020;1(6):2107–16.

18. Ilyas RA, Zuhri MYM, Norrrahim MNF, Misenan MSM, Jenol MA, Samsudin SA, et al. Natural Fiber-Reinforced Polycaprolactone Green and Hybrid Biocomposites for Various Advanced Applications. Polymers. 2022 Jan 3;14(1):182.

19. Labouesse C, Tan BX, Agley CC, Hofer M, Winkel AK, Stirparo GG, et al. StemBond hydrogels control the mechanical microenvironment for pluripotent stem cells. Nat Commun. 2021 Oct 21;12(1):6132.

20. Wang X, Rivera-Bolanos N, Jiang B, Ameer GA. Advanced Functional Biomaterials for Stem Cell Delivery in Regenerative Engineering and Medicine. Adv Funct Mater. 2019;29(23):1809009.

21. Yin S, Cao Y. Hydrogels for Large-Scale Expansion of Stem Cells. Acta Biomater. 2021 Jul 1;128:1–20.

22. Broguiere N, Isenmann L, Hirt C, Ringel T, Placzek S, Cavalli E, et al. Growth of Epithelial Organoids in a Defined Hydrogel. Adv Mater. 2018;30(43):1801621.

23. Ye S, Boeter JWB, Mihajlovic M, van Steenbeek FG, van Wolferen ME, Oosterhoff LA, et al. A Chemically Defined Hydrogel for Human Liver Organoid Culture. Adv Funct Mater. 2020;30(48):2000893.

24. Domogatskaya A, Rodin S, Boutaud A, Tryggvason K. Laminin-511 but Not -332, -111, or -411 Enables Mouse Embryonic Stem Cell Self-Renewal In Vitro. STEM CELLS. 2008;26(11):2800–9.

25. Horejs CM, Serio A, Purvis A, Gormley AJ, Bertazzo S, Poliniewicz A, et al. Biologically-active laminin-111 fragment that modulates the epithelial-to-mesenchymal transition in embryonic stem cells. Proc Natl Acad Sci U S A. 2014 Apr 22;111(16):5908–13.

1016 26. Li L, Arman E, Ekblom P, Edgar D, Murray P, Lonai P. Distinct GATA6- and laminin-dependent
1017 mechanisms regulate endodermal and ectodermal embryonic stem cell fates. Dev Camb Engl.
1018 2004 Nov;131(21):5277–86.

1019 27. Ong J, Serra MP, Segal J, Cujba AM, Ng SS, Butler R, et al. Imaging-Based Screen Identifies
1020 Laminin 411 as a Physiologically Relevant Niche Factor with Importance for i-Hep Applications.
1021 Stem Cell Rep. 2018 Mar 13;10(3):693–702.

1022 28. Borowski M, Giovino-Doherty M, Ji L, Shi MJ, Smith KP. Basic pluripotent stem cell culture
1023 protocols. In: Laning J, editor. StemBook [Internet]. Cambridge (MA): Harvard Stem Cell Institute;
1024 2008 [cited 2023 May 13]. Available from: http://www.ncbi.nlm.nih.gov/books/NBK133258/

1025 29. Stem Cell Culture Guide [Internet]. [cited 2023 May 13]. Available from:
1026 https://www.atcc.org/resources/culture-guides/stem-cell-culture-guide

1027 30. Goetzke R, Keijdener H, Franzen J, Ostrowska A, Nüchtern S, Mela P, et al. Differentiation of
1028 Induced Pluripotent Stem Cells towards Mesenchymal Stromal Cells is Hampered by Culture in 3D
1029 Hydrogels. Sci Rep. 2019 Oct 30;9(1):15578.

1030 31. Jones M, Gabriel DA. Influence of the subendothelial basement membrane components on
1031 fibrin assembly. Evidence for a fibrin binding site on type IV collagen. J Biol Chem. 1988 May
1032 25;263(15):7043–8.

1033 32. Marcinczyk M, Elmashhady H, Talovic M, Dunn A, Bugis F, Garg K. Laminin-111 enriched
1034 fibrin hydrogels for skeletal muscle regeneration. Biomaterials. 2017 Oct;141:233–42.

1035 33. Woodcock-Mitchell J, Mitchell JJ, Low RB, Kieny M, Sengel P, Rubbia L, et al. Alpha-smooth
1036 muscle actin is transiently expressed in embryonic rat cardiac and skeletal muscles. Differ Res Biol
1037 Divers. 1988 Dec;39(3):161–6.

1038 34. Maroof AM, Keros S, Tyson JA, Ying SW, Ganat YM, Merkle FT, et al. Directed differentiation
1039 and functional maturation of cortical interneurons from human embryonic stem cells. Cell Stem
1040 Cell. 2013 May 2;12(5):559–72.

1041 35. Chambers SM, Fasano CA, Papapetrou EP, Tomishima M, Sadelain M, Studer L. Highly
1042 efficient neural conversion of human ES and iPS cells by dual inhibition of SMAD signaling. Nat
1043 Biotechnol. 2009 Mar;27(3):275–80.

1044 36. Hofrichter M, Nimtz L, Tigges J, Kabiri Y, Schröter F, Royer-Pokora B, et al. Comparative
1045 performance analysis of human iPSC-derived and primary neural progenitor cells (NPC) grown as
1046 neurospheres in vitro. Stem Cell Res. 2017 Dec;25:72–82.

1047 37. Ladiwala U, Basu H, Mathur D. Assembling Neurospheres: Dynamics of Neural
1048 Progenitor/Stem Cell Aggregation Probed Using an Optical Trap. PLoS ONE. 2012 Jun
1049 5;7(6):e38613.

1050 38. Kim HJ, Lee E, Nam M, Chung JK, Joo S, Nam Y, et al. Contribution of Extracellular Matrix
1051 Component Landscapes in the Adult Subventricular Zone to the Positioning of Neural
1052 Stem/Progenitor Cells. Exp Neurobiol. 2021 Aug 31;30(4):275–84.

1053 39. Ramli MNB, Lim YS, Koe CT, Demircioglu D, Tng W, Gonzales KAU, et al. Human Pluripotent
1054 Stem Cell-Derived Organoids as Models of Liver Disease. Gastroenterology. 2020
1055 Oct;159(4):1471-1486.e12.

1056 40. Maepa SW, Ndlovu H. Advances in generating liver cells from pluripotent stem cells as a tool
1057 for modeling liver diseases. STEM CELLS. 2020;38(5):606–12.

1058 41. Ang LT, Tan AKY, Autio MI, Goh SH, Choo SH, Lee KL, et al. A Roadmap for Human Liver
1059 Differentiation from Pluripotent Stem Cells. Cell Rep. 2018 Feb;22(8):2190–205.

1060 42. Schafer KA, Eighmy J, Fikes JD, Halpern WG, Hukkanen RR, Long GG, et al. Use of Severity
1061 Grades to Characterize Histopathologic Changes. Toxicol Pathol. 2018 Apr;46(3):256–65.

1062 43. Thuilliez C, Dorso L, Howroyd P, Gould S, Chanut F, Burnett R. Histopathological lesions
1063 following intramuscular administration of saline in laboratory rodents and rabbits. Exp Toxicol
1064 Pathol Off J Ges Toxikol Pathol. 2009 Jan;61(1):13–21.

1065 44. National Toxicology Program [Internet]. [cited 2023 May 24]. Nonneoplastic Lesion Atlas.
1066 Available from: https://ntp.niehs.nih.gov/atlas/nnl

1067 45. Avior Y, Sagi I, Benvenisty N. Pluripotent stem cells in disease modelling and drug discovery.
1068 Nat Rev Mol Cell Biol. 2016 Mar;17(3):170–82.

1069 46. Sozzi E, Kajtez J, Bruzelius A, Wesseler MF, Nilsson F, Birtele M, et al. Silk scaffolding drives
1070 self-assembly of functional and mature human brain organoids. Front Cell Dev Biol. 2022 Oct
1071 14;10:1023279.

1072 47. Hannan NRF, Segeritz CP, Touboul T, Vallier L. Production of hepatocyte like cells from
1073 human pluripotent stem cells. Nat Protoc. 2013 Feb;8(2):430–7.

1074 48. Klaffky E, Williams R, Yao CC, Ziober B, Kramer R, Sutherland A. Trophoblast-specific
1075 expression and function of the integrin alpha 7 subunit in the peri-implantation mouse embryo.
1076 Dev Biol. 2001 Nov 1;239(1):161–75.

1077 49. Pook M, Teino I, Kallas A, Maimets T, Ingerpuu S, Jaks V. Changes in Laminin Expression
1078 Pattern during Early Differentiation of Human Embryonic Stem Cells. PloS One.
1079 2015;10(9):e0138346.

1080 50. Galanakis D, Nuovo G, Spitzer S, Kaplan C, Scharrer I. Fibrinogen mRNA and antigen co-
1081 present in human trophoblasts in situ: possible implications. Thromb Res. 1996 Jan 15;81(2):263–
1082 9.

1083 51. Weisel JW, Litvinov RI. Fibrin Formation, Structure and Properties. Subcell Biochem.
1084 2017;82:405–56.

1085 52. Sánchez-Cortés J, Mrksich M. The platelet integrin alphaIIbbeta3 binds to the RGD and AGD
1086 motifs in fibrinogen. Chem Biol. 2009 Sep 25;16(9):990–1000.

1087 53. Suehiro K, Mizuguchi J, Nishiyama K, Iwanaga S, Farrell DH, Ohtaki S. Fibrinogen binds to
1088 integrin alpha(5)beta(1) via the carboxyl-terminal RGD site of the Aalpha-chain. J Biochem
1089 (Tokyo). 2000 Oct;128(4):705–10.

1090 54. Wondimu Z, Omrani S, Ishikawa T, Javed F, Oikawa Y, Virtanen I, et al. A Novel Monoclonal
1091 Antibody to Human Laminin α5 Chain Strongly Inhibits Integrin-Mediated Cell Adhesion and
1092 Migration on Laminins 511 and 521. PLOS ONE. 2013 Jan 7;8(1):e53648.

1093 55. Ishihara J, Ishihara A, Fukunaga K, Sasaki K, White MJV, Briquez PS, et al. Laminin heparin-
1094 binding peptides bind to several growth factors and enhance diabetic wound healing. Nat
1095 Commun. 2018 Jun 4;9(1):2163.

1096 56. Presser N, Kerr H, Gao T, Begala M, Paschal S, Shoskes DA, et al. Fibrin Glue Injections: A
1097 Minimally Invasive and Cost-Effective Treatment for Post-Renal Transplant Lymphoceles and
1098 Lymph Fistulas. Am J Transplant Off J Am Soc Transplant Am Soc Transpl Surg. 2016
1099 Feb;16(2):694–9.

1100 57. Gandhi JK, Knudsen T, Hill M, Roy B, Bachman L, Pfannkoch-Andrews C, et al. Human
1101 Fibrinogen for Maintenance and Differentiation of Induced Pluripotent Stem Cells in Two
1102 Dimensions and Three Dimensions. Stem Cells Transl Med. 2019 Feb 15;8(6):512–21.

1103 58. Duong H, Wu B, Tawil B. Modulation of 3D fibrin matrix stiffness by intrinsic fibrinogen-
1104 thrombin compositions and by extrinsic cellular activity. Tissue Eng Part A. 2009 Jul;15(7):1865–
1105 76.

1106 59. Frye M, Taddei A, Dierkes C, Martinez-Corral I, Fielden M, Ortsäter H, et al. Matrix stiffness
1107 controls lymphatic vessel formation through regulation of a GATA2-dependent transcriptional
1108 program. Nat Commun. 2018 Apr 17;9(1):1511.

1109 60. Garcia-Abrego C, Zaunz S, Toprakhisar B, Subramani R, Deschaume O, Jooken S, et al.
1110 Towards Mimicking the Fetal Liver Niche: The Influence of Elasticity and Oxygen Tension on
1111 Hematopoietic Stem/Progenitor Cells Cultured in 3D Fibrin Hydrogels. Int J Mol Sci. 2020
1112 Jan;21(17):6367.

1113 61. Chowdhury F, Li Y, Poh YC, Yokohama-Tamaki T, Wang N, Tanaka TS. Soft substrates
1114 promote homogeneous self-renewal of embryonic stem cells via downregulating cell-matrix
1115 tractions. PloS One. 2010 Dec 13;5(12):e15655.

1116 62. Liu J, Tan Y, Zhang H, Zhang Y, Xu P, Chen J, et al. Soft fibrin gels promote selection and
1117 growth of tumourigenic cells. Nat Mater. 2012 Jul 1;11(8):734–41.

1118 63. Genovese P, Patel A, Ziemkiewicz N, Paoli A, Bruns J, Case N, et al. Co-delivery of fibrin-
1119 laminin hydrogel with mesenchymal stem cell spheroids supports skeletal muscle regeneration
1120 following trauma. J Tissue Eng Regen Med. 2021;15(12):1131–43.

1121 64. Ziemkiewicz N, Hilliard GM, Dunn AJ, Madsen J, Haas G, Au J, et al. Laminin-111-Enriched
1122 Fibrin Hydrogels Enhance Functional Muscle Regeneration Following Trauma. Tissue Eng Part A.
1123 2022 Apr;28(7–8):297–311.

1124 65. Nam K, Maruyama CL, Wang CS, Trump BG, Lei P, Andreadis ST, et al. Laminin-111-derived
1125 peptide conjugated fibrin hydrogel restores salivary gland function. PLOS ONE. 2017 Nov
1126 2;12(11):e0187069.

1127 66. Huch M, Boj SF, Clevers H. Lgr5(+) liver stem cells, hepatic organoids and regenerative
1128 medicine. Regen Med. 2013 Jul;8(4):385–7.

1129 67. Jha R, Xu RH, Xu C. Efficient Differentiation of Cardiomyocytes from Human Pluripotent Stem
1130 Cells with Growth Factors. Methods Mol Biol Clifton NJ. 2015;1299:115–31.

1131 68. Rhee YH, Puspita L, Sulistio YA, Kim SW, Vidyawan V, Elvira R, et al. Efficient Neural
1132 Differentiation of hPSCs by Extrinsic Signals Derived from Co-cultured Neural Stem or Precursor
1133 Cells. Mol Ther. 2019 Jul 3;27(7):1299–312.

1134 69. Lancaster MA, Corsini NS, Wolfinger S, Gustafson EH, Phillips AW, Burkard TR, et al. Guided
1135 self-organization and cortical plate formation in human brain organoids. Nat Biotechnol. 2017
1136 Jul;35(7):659–66.

1137 70. Dhawan A, Puppi J, Hughes RD, Mitry RR. Human hepatocyte transplantation: current
1138 experience and future challenges. Nat Rev Gastroenterol Hepatol. 2010 May;7(5):288–98.

1139 71. Forbes SJ, Gupta S, Dhawan A. Cell therapy for liver disease: From liver transplantation to
1140 cell factory. J Hepatol. 2015 Apr;62(1 Suppl):S157-169.

1141 72. Dhawan A, Chaijitraruch N, Fitzpatrick E, Bansal S, Filippi C, Lehec SC, et al. Alginate
1142 microencapsulated human hepatocytes for the treatment of acute liver failure in children. J
1143 Hepatol. 2020 May;72(5):877–84.

1144 73. Zhao T, Zhang ZN, Rong Z, Xu Y. Immunogenicity of induced pluripotent stem cells. Nature.
1145 2011 May 13;474(7350):212–5.

1146 74. Tricot T, Verfaillie CM, Kumar M. Current Status and Challenges of Human Induced
1147 Pluripotent Stem Cell-Derived Liver Models in Drug Discovery. Cells. 2022 Jan;11(3):442.

1148 75. Mallanna SK, Duncan SA. Differentiation of hepatocytes from pluripotent stem cells. Curr
1149 Protoc Stem Cell Biol. 2013 Sep 20;26:1G.4.1-1G.4.13.

1150 76. Cheung C, Bernardo AS, Pedersen RA, Sinha S. Directed differentiation of embryonic origin-
1151 specific vascular smooth muscle subtypes from human pluripotent stem cells. Nat Protoc. 2014
1152 Apr;9(4):929–38.

1153 77. Burridge PW, Holmström A, Wu JC. Chemically Defined Culture and Cardiomyocyte
1154 Differentiation of Human Pluripotent Stem Cells. Curr Protoc Hum Genet. 2015 Oct 6;87:21.3.1-
1155 21.3.15.

1156 78. Tyzack GE, Sitnikov S, Barson D, Adams-Carr KL, Lau NK, Kwok JC, et al. Astrocyte response to
1157 motor neuron injury promotes structural synaptic plasticity via STAT3-regulated TSP-1 expression.
1158 Nat Commun. 2014 Jul 11;5:4294.

1159 79. Katarivas Levy G, Ong J, Birch MA, Justin AW, Markaki AE. Albumin-Enriched Fibrin Hydrogel
1160 Embedded in Active Ferromagnetic Networks Improves Osteoblast Differentiation and Vascular
1161 Self-Organisation. Polymers. 2019 Oct 24;11(11):1743.

1162 80. Varley MC, Neelakantan S, Clyne TW, Dean J, Brooks RA, Markaki AE. Cell structure, stiffness
1163 and permeability of freeze-dried collagen scaffolds in dry and hydrated states. Acta Biomater.
1164 2016 Mar;33:166–75.

1165 81. Kitajima M, Kimura A, Suzuki H. Cutting Edge: Nqo1 Regulates Irritant Contact
1166 Hypersensitivity against Croton Oil through Maintenance of Dendritic Epidermal T Cells. J
1167 Immunol Baltim Md 1950. 2018 Mar 1;200(5):1555–9.

1168

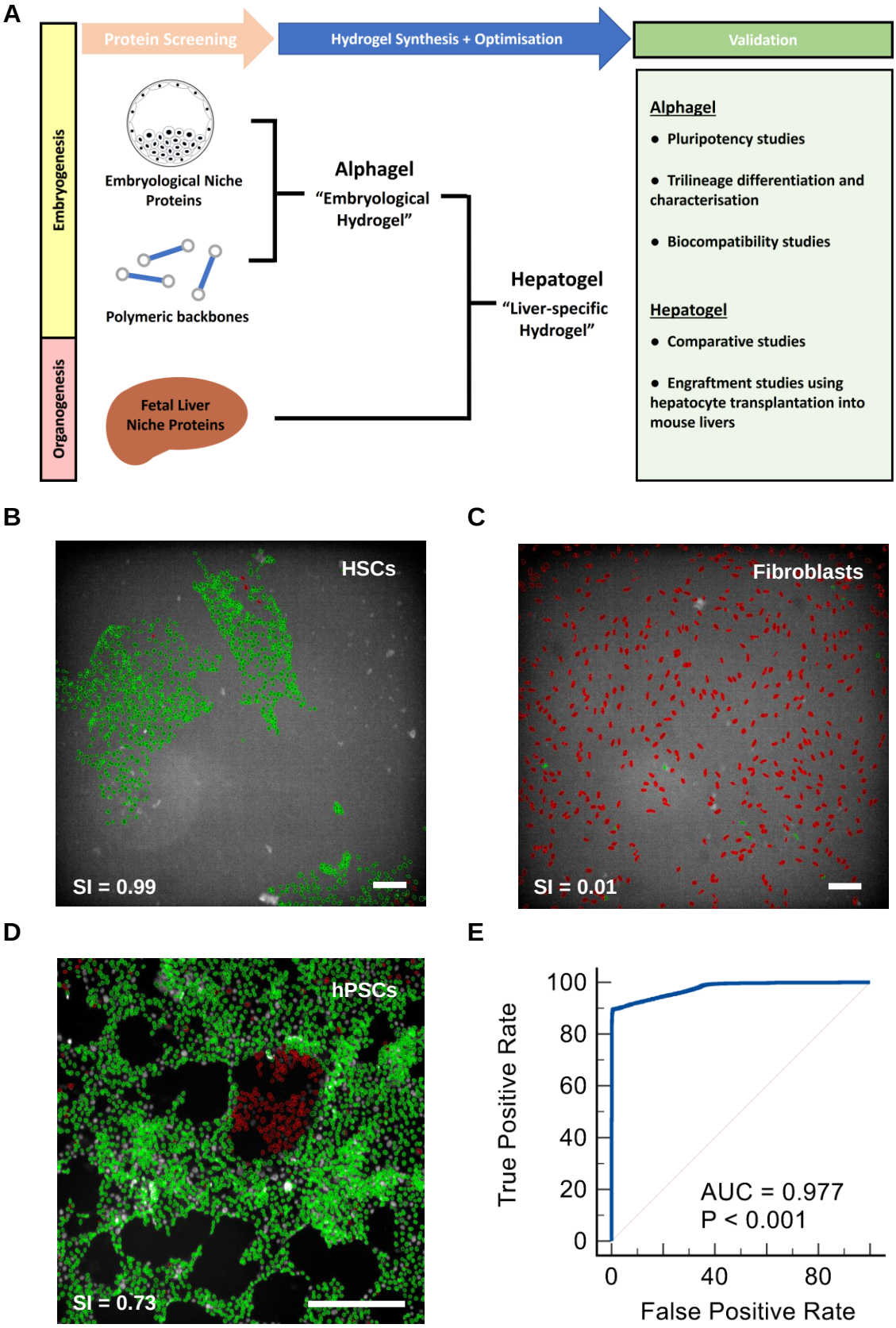

Figure 1. A) Schematic of workflow. B) Automated pipeline identifying hPSC colonies as pluripotent stem cells; green = positive selection by machine learning, scale bar = 100 µm. C) Machine learning identifying human fibroblasts as non-pluripotent cells (red); scale bar = 100 µm. D) Machine learning discriminating undifferentiated hPSCs (green) from spontaneously differentiated hPSCs (red) after intentionally extended culture to trigger spontaneous differentiation (Day 9), scale bar = 200 µm. E) A Receiver Operator Characteristic curve showing excellent discriminatory performance of our machine-learning platform with an Area Under the Curve (AUC) of 0.977.

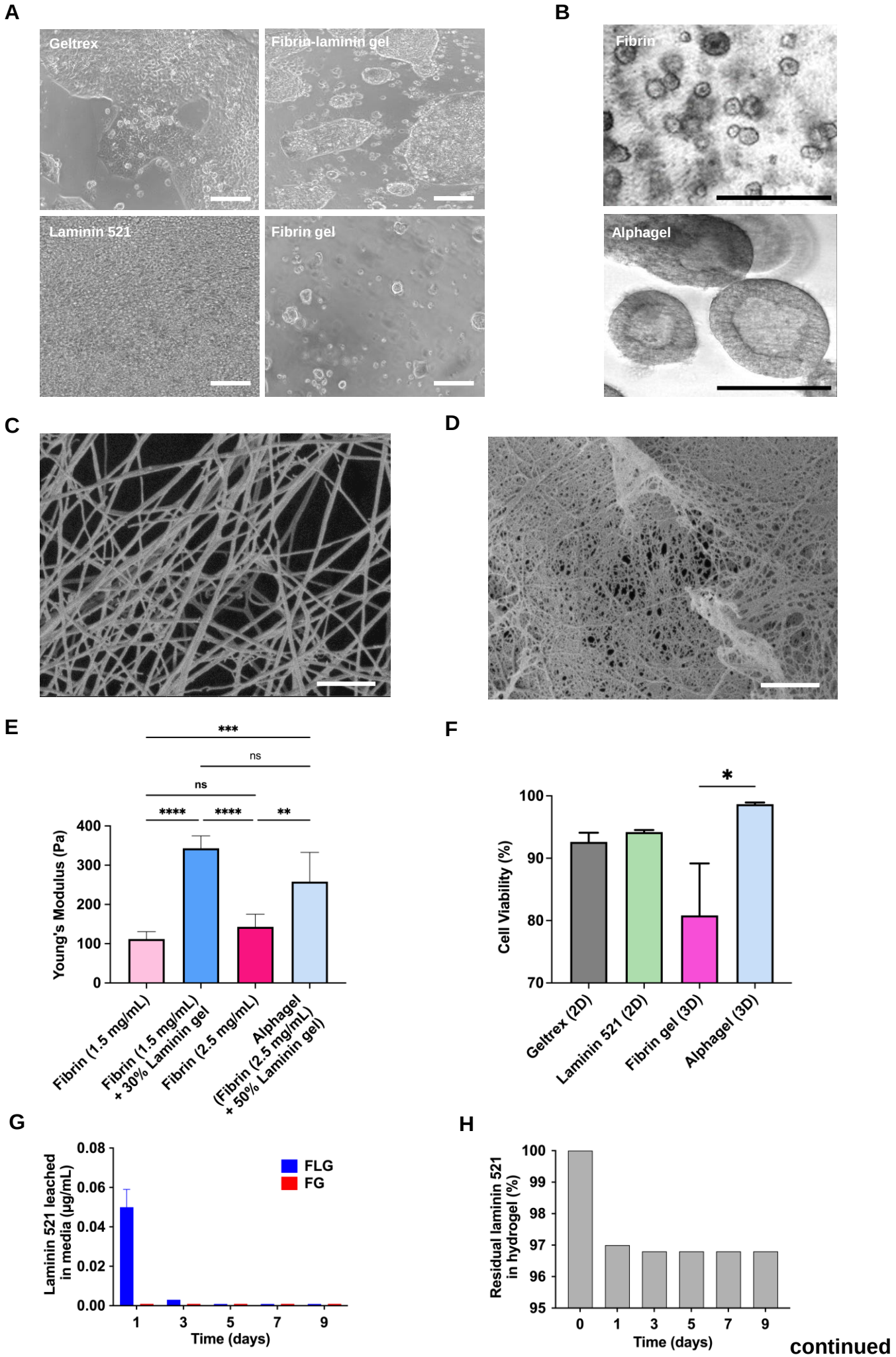
A
Geltrex
Fibrin-laminin gel
Laminin 521
Fibrin gel
B
Fibrin
Alphagel
C
D
E
***
ns
ns
****
****
**
Young's Modulus (Pa)
400
300
200
100
0
Fibrin (1.5 mg/mL)
Fibrin (1.5 mg/mL) + 30% Laminin gel
Fibrin (2.5 mg/mL)
Alphagel (Fibrin (2.5 mg/mL) + 50% Laminin gel)
F
*
Cell Viability (%)
100
90
80
70
Geltrex (2D)
Laminin 521 (2D)
Fibrin gel (3D)
Alphagel (3D)
G
Laminin 521 leached in media (µg/mL)
0.08
0.06
0.04
0.02
0.00
FLG
FG
1
3
5
7
9
Time (days)
H
Residual laminin 521 in hydrogel (%)
100
99
98
97
96
95
0
1
3
5
7
9
Time (days)

continued

Figure 2. A) hPSC confluence in 2D growth factor reduced Matrigel (Geltrex), Laminin 521, fibrin-laminin hydrogel, and fibrin gel after 4 days. Scale bar = 100 µm. B) hPSCs cultured in 3D hydrogels. Top panel: Fibrin (5 mg/mL) gel. Bottom panel: Alphagel containing structures resembling embryoid bodies, scale bar = 200 µm. SEM of (C) fibrin gel and (D) Alphagel, scale bar = 1 µm, magnification 20K X, iProbe = 13 pA, 2.00 kV, WD = 4.4 mm for both images. E) Young's moduli in hydrogels with varying fibrin and laminin concentrations. One-way ANOVA; ** = $p < 0.01$, *** = $p < 0.001$, and **** = $p < 0.0001$. F) Cell viability of hPSCs cultured in Alphagel, fibrin-only hydrogels, and 2D standard substrates. Mean ± S.E.M displayed. t-test; * = $p < 0.05$. G) ELISA of Laminin 521 in culture media used with acellular Alphagel and H) the calculated amount of fibrin-bound laminin over time.

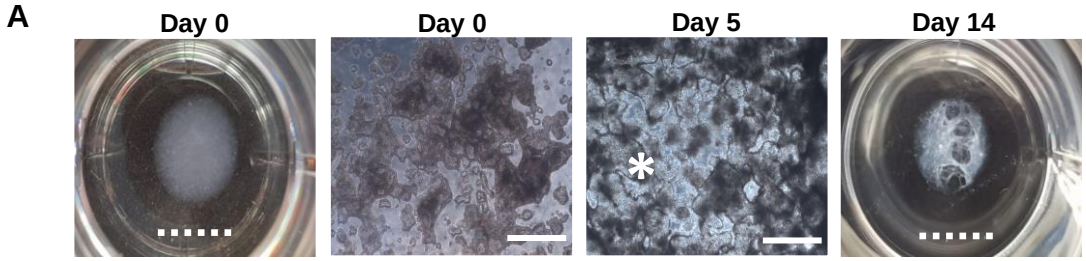
A
Day 0
Day 0
Day 5
Day 14

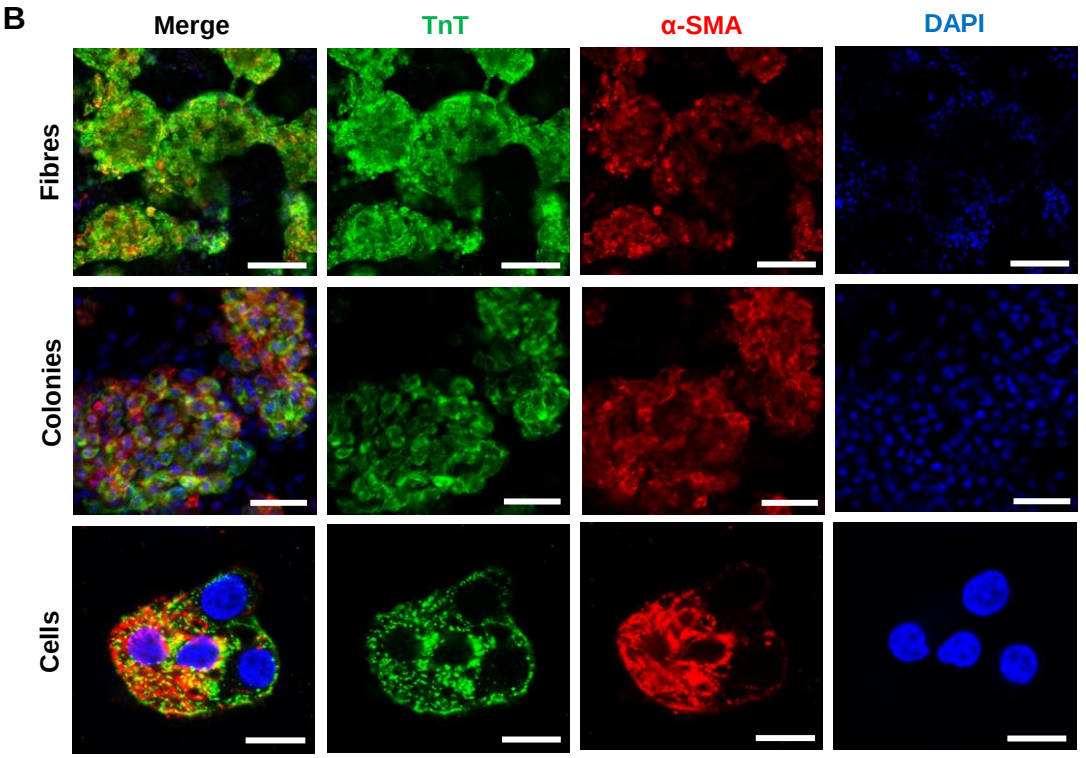
B
Merge
TnT
α-SMA
DAPI
Fibres
Colonies
Cells

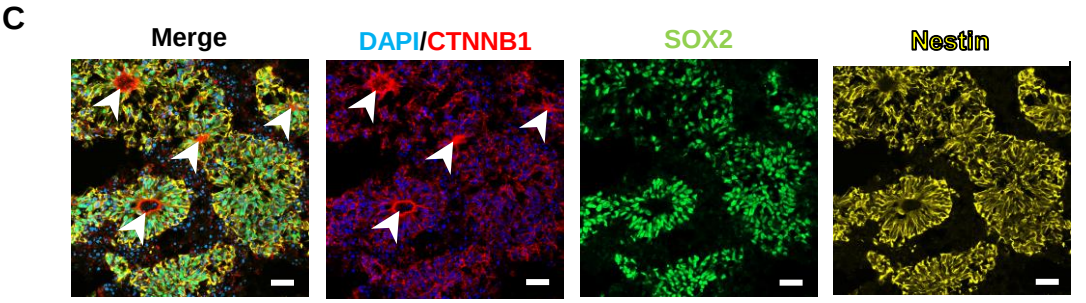
C
Merge
DAPI/CTNNB1
SOX2
Nestin

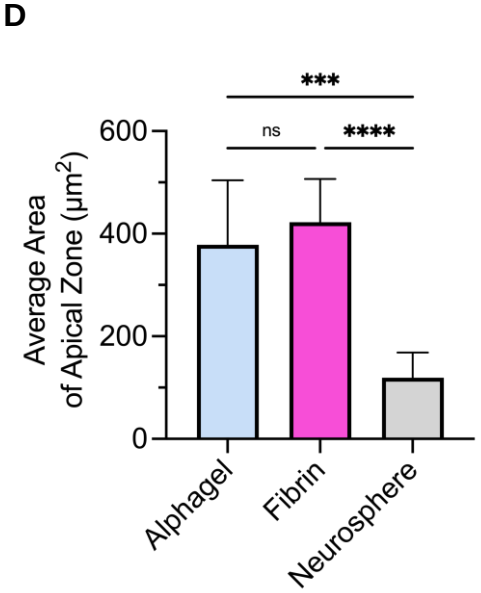
D
***
ns
****
600
400
200
0
Average Area of Apical Zone (μm²)
Alphagel
Fibrin
Neurosphere

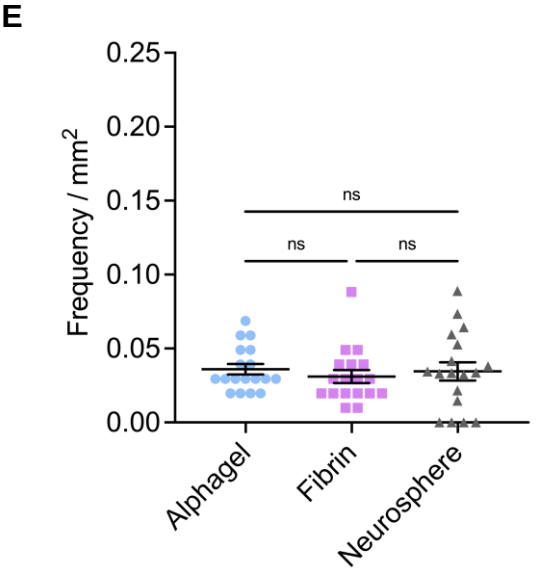
E
0.25
0.20
0.15
0.10
0.05
0.00
Frequency / mm²
ns
ns
ns
Alphagel
Fibrin
Neurosphere

continued

Figure 3: A) Macroscopic and microscopic appearances of cells in Alphagel. Contractile cardiomyocyte colonies (*) are visible by Day 6. By Day 14 contractile tissue resembling trabeculae carnae is observed. Scale bar: full line = 100 µm, dotted line = 1 cm. B) Troponin T (TnT), alpha-smooth muscle actin (α-SMA), and DAPI in cardiomyocytes cultured with Alphagel. Scale bar = 100 µm (fibres), 50 µm (colonies), and 20 µm (cells). C) Alphagel-derived neuroepithelia expressing β catenin (CTNNB1), SOX2 and Nestin. Arrows indicate apical zones demarcated by β catenin. Scale bar = 100 µm. D) Average lumen area of neuroepithelia in Alphagel, fibrin gel, and neurospheres (Matrigel). E) Frequency of polarized puncta per mm^2. The Kruskal-Wallis test was used for (D) and (E). *** = $p < 0.001$, and **** = $p < 0.0001$.

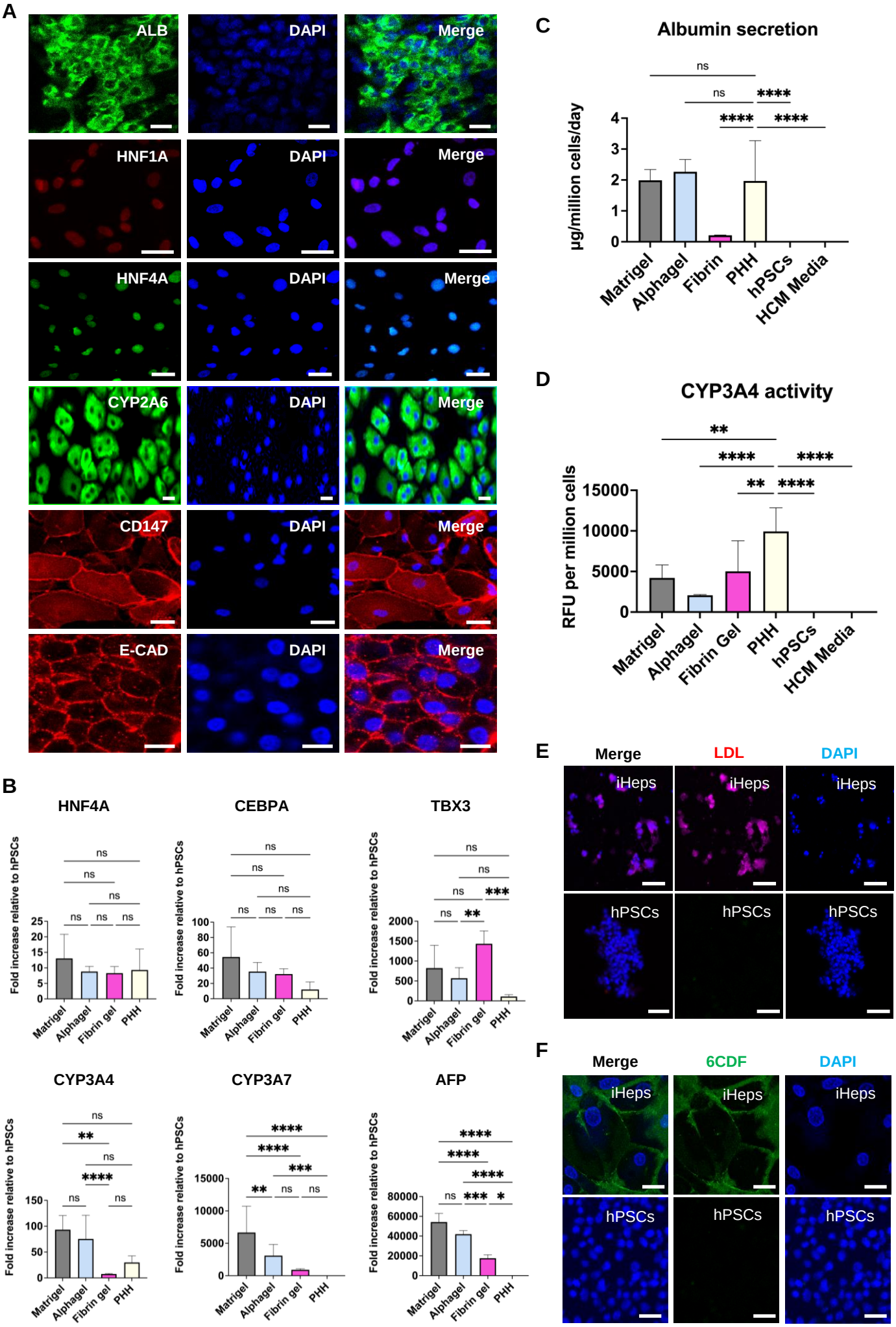
A
ALB
DAPI
Merge
HNF1A
HNF4A
CYP2A6
CD147
E-CAD
B
HNF4A
CEBPA
TBX3
CYP3A4
CYP3A7
AFP
Fold increase relative to hPSCs
Matrigel
Alphagel
Fibrin gel
PHH
C
Albumin secretion
µg/million cells/day
Fibrin
hPSCs
HCM Media
D
CYP3A4 activity
RFU per million cells
Fibrin Gel
E
LDL
iHeps
F
6CDF

Figure 4: A) Key hepatocyte markers in Alphagel-derived iHeps. ALB = albumin, HNF = Hepatocyte Nuclear Factor, CYP2A6 = Cytochrome 2A6, CD147 = Cluster of Differentiation protein 147, and E-CAD = E-cadherin. Scale bar = 25 µm. B) Key hepatocyte markers by gene expression (qPCR). C) Albumin secretion (ELISA) and D) CYP3A4 activity (P450-Glo™) in PHH vs iHeps cultured in various gels (Day 22). HCM = Hepatocyte Culture Media (Lonza). (E) LDL uptake (red) in Alphagel-derived iHeps versus hPSCs. Scale bar = 100 µm. F) CDFDA secretion (green) in Alphagel-derived iHeps vs hPSCs. Top panel scale bar = 20 µm, bottom panel scale bar = 50 µm. One-way ANOVA was used; * = $p < 0.05$, ** = $p < 0.01$, *** = $p < 0.001$, and **** = $p < 0.0001$.

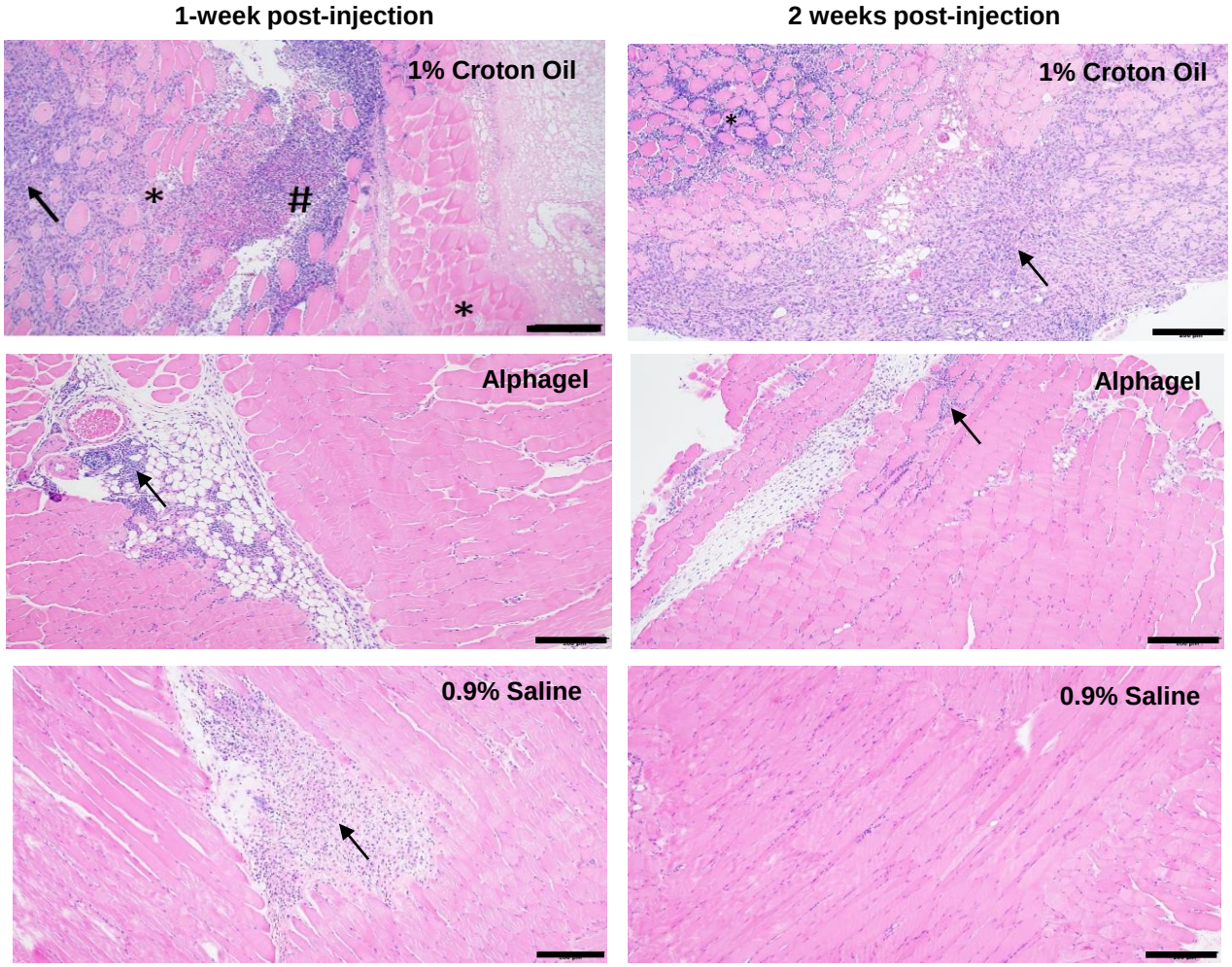

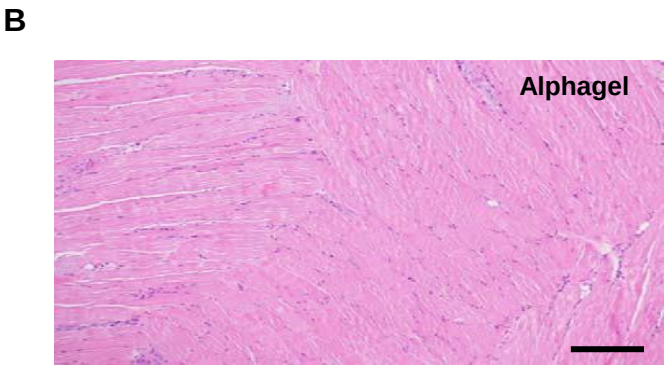

C

Inflammation Severity

	Week 1: Grade (Score)	Week 2: Grade (Score)	Weeks 4-6: Grade (Score)
1% Croton oil	Severe (13.3 ± 2.5)	Severe (14.7 ± 4.0)	Culled (N/A)
Alphagel	Mild (4.3 ± 1.5)	Minimal (3.3 ± 0.6)	Normal (0)
0.9% Saline	Minimal (0.25 ± 0.05)	Normal (0)	Normal (0)

Figure 5: A) H&E stains of sites injected with 1% Croton Oil, Alphagel, and 0.9% Saline at 1 and 2 weeks. Black arrow denotes areas of granulation and inflammation, * denotes necrotic and degenerating muscle fibres, and # denotes supportive changes around affected muscle fibres. Scale bar = 200 µm. B) H&E stain of Alphagel injection site after 6 weeks showing complete resolution of previously mild inflammation. Scale bar = 200 µm. C) Histological grade and scores of injection sites over 6 weeks. One-way ANOVA; * = $p < 0.05$, ** = $p < 0.01$, *** = $p < 0.001$, and **** = $p < 0.0001$.

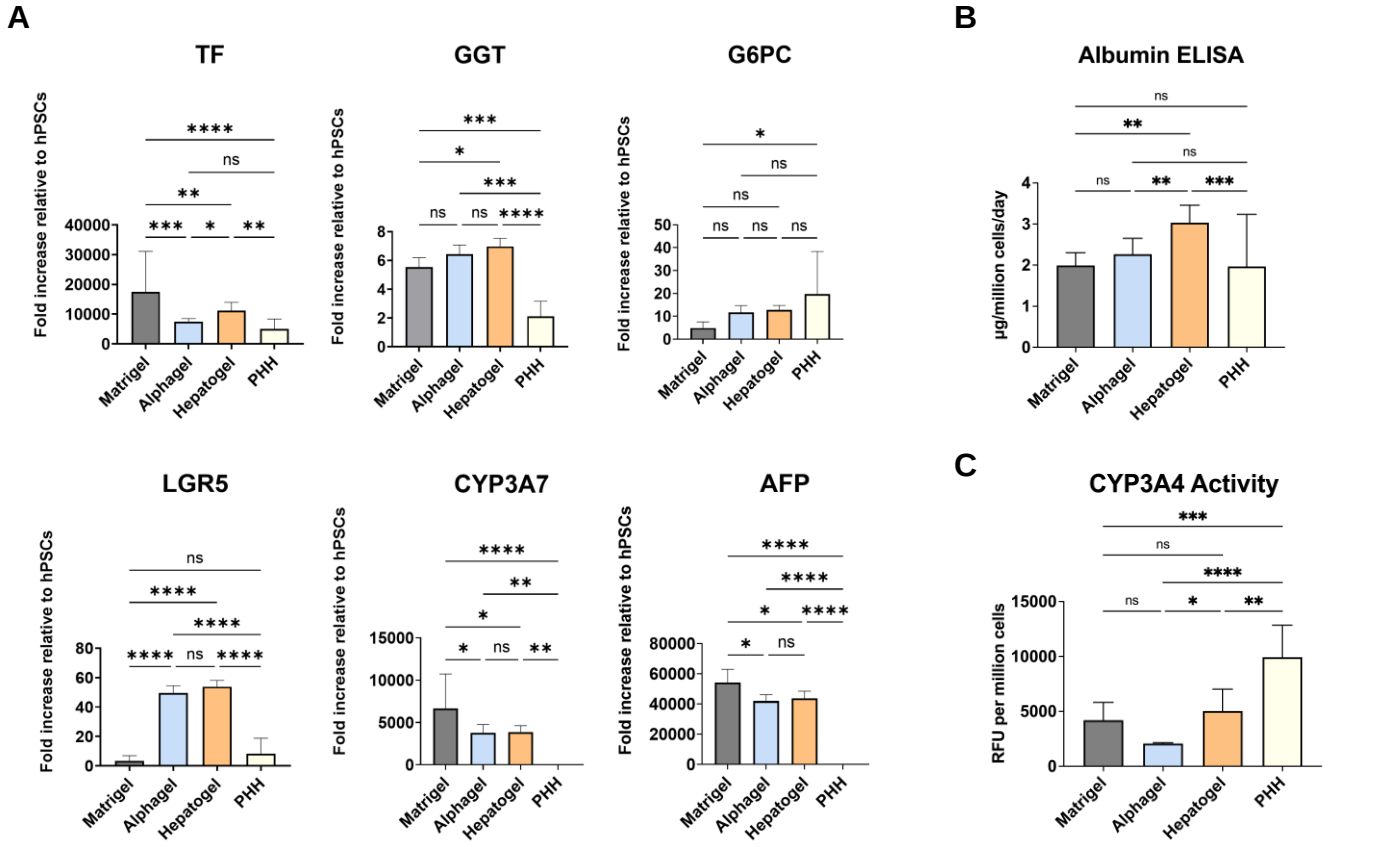
A
TF
GGT
G6PC
LGR5
CYP3A7
AFP
Fold increase relative to hPSCs
Matrigel
Alphagel
Hepatogel
PHH
B
Albumin ELISA
µg/million cells/day
C
CYP3A4 Activity
RFU per million cells

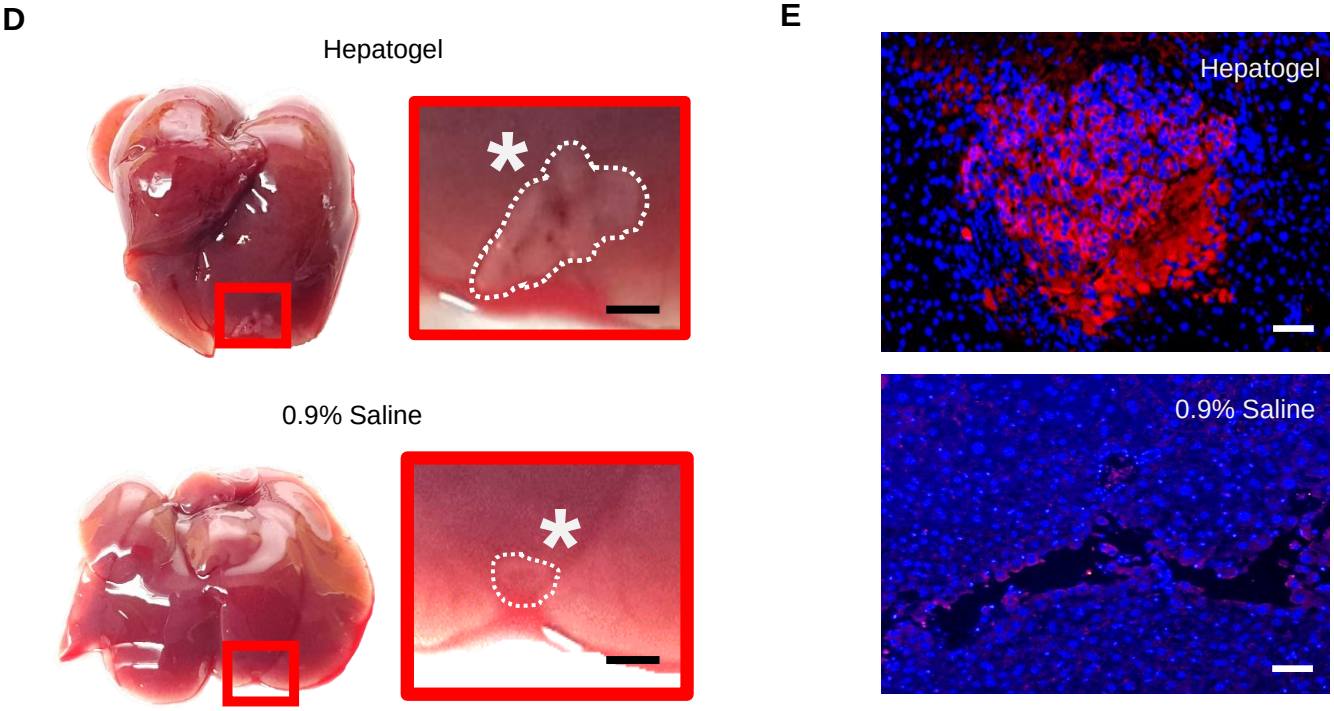
D
Hepatogel
0.9% Saline
E
Hepatogel
0.9% Saline

continued

F

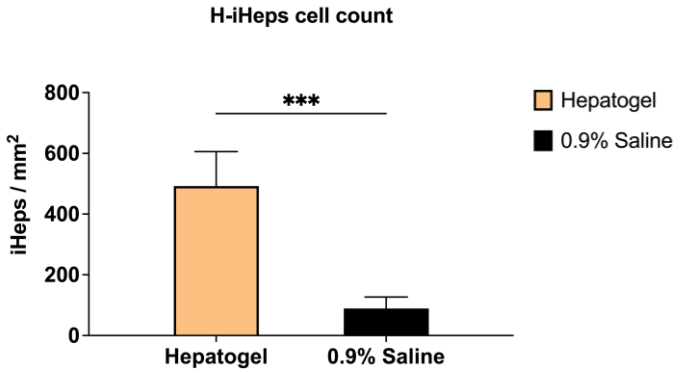

G

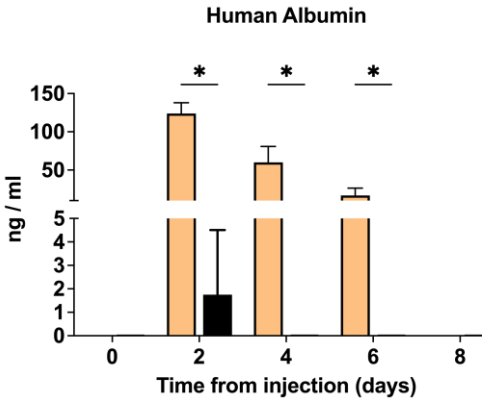

Figure 6: A) Differentially expressed genes in iHeps; Hepatologel, Alphagel, Matrigel, and adult primary human hepatocytes (PHH). B) Albumin ELISA of culture media and C) Luciferin-based measure of CYP3A4 activity; 2 days after completion of iHep differentiation and 2 days after plating PHH. One-way ANOVA; * = $p < 0.05$, ** = $p < 0.01$, *** = $p < 0.001$, and **** = $p < 0.0001$. D) Mouse livers 3 days after intra-hepatic injection with H-iHeps in Hepatogel and 0.9% saline. Red box = area magnified. * = site of injection, dotted white lines demarcate engrafted cell mass, scale bar = 1 mm. E) Human albumin (stained red) in engrafted iHeps 3 days after intra-hepatic injection. Scale bar = 100 µm. F) H-iHeps identified by albumin staining on liver histology 3 days after intra-hepatic injection. G) ELISA of mouse serum for human albumin after injection with H-iHeps in Hepatogel and 0.9% saline over time. Day 0 = serum levels before injection. T-test; *** = $p < 0.001$, and **** = $p < 0.0001$.